

CE-DYNAM (v1), a spatially explicit, process-based carbon erosion scheme for the use in Earth system models

Victoria Naipal^{1,2}, Ronny Lauerwald³, Philippe Ciais², Bertrand Guenet², Yilong Wang²

¹Ludwig-Maximilians University, Munich, Germany

²Laboratoire des Sciences des Sciences du Climat et de l'Environnement, CEA CNRS UVSQ, Gif-sur-Yvette 91191, France

³Department of Geoscience, Environment and Society, Université Libre de Bruxelles, Brussels, Belgium

Correspondence : Victoria Naipal (vnaipal24@gmail.com)

Abstract. Soil erosion by rainfall and runoff is an important process behind the redistribution of soil organic carbon (SOC) over land, hereby impacting the exchange of carbon (C) between land, atmosphere and rivers. However, the net role of soil erosion in the global C cycle is still unclear as it involves small-scale SOC removal, transport and re-deposition processes that can only be addressed over selected small regions with complex models and measurements. This leads to uncertainties in future projections of SOC stocks and complicates the evaluation of strategies to mitigate climate change through increased SOC sequestration.

In this study we present the parsimonious process-based Carbon Erosion DYNAMics model (CE-DYNAM) that links sediment dynamics resulting from water erosion with the C cycle along a cascade of hillslopes, floodplains and rivers. The model simulates horizontal soil and C transfers triggered by erosion across landscapes and the resulting changes in land-atmosphere CO₂ fluxes at a resolution of about 8 km at the catchment scale. CE-DYNAM is the result of the coupling of a previously developed coarse-resolution sediment budget model and the ecosystem C cycle and erosion removal model derived from the ORCHIDEE land surface model. CE-DYNAM is driven by spatially explicit historical land use change, climate forcing, and global atmospheric CO₂ concentrations affecting ecosystem productivity, erosion rates and residence times of sediment and C in deposition sites. The main features of CE-DYNAM are (1) the spatially explicit simulation of sediment and C fluxes linking hillslopes and floodplains, (2) the relative low number of parameters that allow running the model at large spatial scales and over long-time scales, and (3) its compatibility with global land surface models, hereby, providing opportunities to study the effect of soil erosion under global changes.

We present the model structure, concepts, limitations and evaluation at the scale of the Rhine catchment for the period 1850-2005 AD. Model results are validated against independent estimates of gross and net soil and C erosion rates, and the spatial variability of SOC stocks from high-resolution modeling studies and observational datasets. We show that despite local differences, the resulting soil and C erosion rates, and SOC stocks from CE-DYNAM are comparable to high-resolution estimates and observations at sub-basin level.

35

36 We find that soil erosion mobilized around $66 \pm 28 \text{ Tg}$ (10^{12} g) of C under changing climate and land use over the
37 non-Alpine region of the Rhine catchment, assuming that the erosion loop of the C cycle was in near steady-state by 1850.
38 This caused a net C sink equal to 2.1 - 2.7% of the Net Primary Productivity of the non-Alpine region over 1850-2005 AD.
39 This sink is a result of the dynamic replacement of C on eroding sites that increases in this period due to rising atmospheric
40 CO_2 concentrations enhancing the litter C input to the soil from primary production.

41

42 **Keywords.** soil erosion; regional carbon cycle; carbon sink; Rhine catchment; regional modelling

43

44 **1 Introduction**

45

46 Soils contain more carbon (C) than the atmosphere and living biomass together. Relatively small disturbances
47 (anthropogenic or natural) to soil C pools over large areas could add up to substantial C emissions (Ciais et al., 2013). With
48 the removal of natural vegetation and the introduction of mechanized agriculture, humans have accelerated soil erosion
49 rates. Over the last two to three decades, studies have shown that water erosion (soil erosion by rainfall and runoff)
50 amplified by human activities has substantially impacted the terrestrial C budget (Doetterl et al., 2012; Lal, 2003; Lugato et
51 al., 2018; Van Oost et al., 2007, 2012; Stallard, 1998; Wang et al., 2017). However, the net effect of water erosion on the C
52 cycle at regional to global scale is still under debate. This leads to uncertainties in the future projections of the soil organic
53 C (SOC) reservoir, and complicates the evaluation of strategies to mitigate climate change by increased SOC sequestration.
54 The study of Stallard (1998) was one of the first to show that water erosion does not only lead to additional C emissions
55 but can also sequester C due to the photosynthetic replacement of SOC at eroding sites and the stabilization of SOC in
56 deeper layers at burial sites. The study of van Oost et al. (2007) was the first to confirm the importance of the sequestration
57 of SOC by agricultural erosion at global scale using isotope tracers. Wang et al. (2017) gathered data on SOC profiles from
58 erosion and deposition sites and confirmed that water erosion on agricultural land that started from the early/middle
59 Holocene has caused a large net global land C sink. Other studies, however, argue that soil erosion is a net C source to the
60 atmosphere due to increased SOC decomposition following soil aggregate breakdown during transport and at deposition
61 sites (Lal et al, 2003; Lugato et al., 2018). Most studies modeling soil erosion and its net effect on SOC dynamics at global
62 scale, however, did not account for the full range of complex effects of climate change, CO_2 fertilization increasing
63 productivity and potentially soil C inputs, harvest of biomass, land use change, and changes in cropland management
64 (Borrelli et al., 2018; Doetterl et al., 2012; Chappell et al., 2016; Lugato et al., 2018; Van Oost et al., 2007; Wang et al.,
65 2017). In addition, models used at large spatial scales mainly focus on hillslopes and removal processes and neglect
66 floodplain sediment and SOC dynamics (Borrelli et al., 2018; Chappell et al., 2016; Lugato et al., 2018; Van Oost et al.,
67 2007). This can lead to substantial biases in the assessment of net effects of SOC erosion at catchment scale because
68 floodplains can store substantial amounts of sediment and C (Berhe et al., 2007; Hoffmann et al., 2013a,b). Studies

69 addressing long-term large-scale sediment yield from hillslopes and floodplains, such as Pelletier et al. (2012), do not
70 explicitly account for the redistribution of sediment and SOC over land.

71
72 Furthermore, soil erosion is one of the main contributors to particulate organic carbon (POC) fluxes in rivers and C export
73 to the coastal ocean. The riverine POC fluxes are usually much smaller than the SOC erosion fluxes, because only a small
74 fraction of eroded material is entering the river network, while POC losses occur in the river network and due to
75 decomposition and burial in floodplains and in benthic sediments (Tan et al., 2017; Galy et al., 2015). Therefore,
76 uncertainties in large-scale SOC erosion rates will lead to even larger uncertainties in lateral C fluxes between land and
77 ocean for past and future scenarios estimated by global empirical models on riverine C export (Ludwig and Probst, 1998;
78 Mayorga et al., 2010).

79
80 To address these knowledge gaps, we present a parsimonious process-based Carbon Erosion Dynamics Model
81 (CE-DYNAM), which integrates sediment dynamics resulting from water erosion with the SOC dynamics at the regional
82 scale. The SOC dynamics are calculated consistently with drivers of land use change, CO₂ and climate change by a
83 process-based land surface model (LSM), with a simplified reconstruction of the last century increase of crop productivity.
84 This modelling approach consists of a global sediment budget model coupled to the SOC removal, input, and
85 decomposition processes diagnosed from the ORCHIDEE global LSM in an offline setting (Naipal et al., 2018). The main
86 aim of our study is to quantify the horizontal transport of sediment and C along the continuum of hillslopes and
87 floodplains, and at the same time analyze its impacts on the land-atmosphere C exchange. We validate the new model with
88 regional observations and high-resolution modelling results of the Rhine catchment. It should be noted here that the
89 structure of CE-DYNAM is designed in a way that the model can be adapted easily to other large catchments after
90 calibrating the model parameters to the specific environmental conditions in those catchments. We also discuss the model
91 uncertainties and the sensitivity of the model to changes in key model parameters and assumptions made. In the next
92 sections we give a detailed overview of the CE-DYNAM model structure, the coupling of erosion, deposition and transport
93 with the coarse-resolution SOC dynamics of ORCHIDEE, model application and validation for the non-Alpine region of
94 the Rhine catchment, and its potentials and limitations.

95 96 **2 Methods**

97 98 **2.1 General model description**

99
100 CE-DYNAM version 1 (v1) is the result of coupling a large-scale erosion and sediment budget model (Naipal et al., 2016)
101 with the SOC scheme of the ORCHIDEE LSM (Krinner et al., 2005). The most important features of the model are (1) the
102 spatially explicit simulation of lateral sediment and C transport fluxes over land linking hillslopes and floodplains, (2)
103 consistent simulation of vertical C fluxes coupled with horizontal transport, (3) the low number of parameters compared to

104 other C erosion models that operate at a high spatial resolution (Lugato et al., 2018; Billings et al., 2019) that allows
105 running the model at large spatial scales and over time-scales up to several thousands of years, (4) the generic input fields
106 for application to any region or catchment, and (5) compatibility with LSMs.

107
108 In the ORCHIDEE LSM, terrestrial C is represented by eight biomass pools, four litter pools and three SOC pools. Each of
109 the pools varies in space, time and over the twelve Plant Functional Types (PFTs). An extra PFT is used to represent bare
110 soil. Anthropogenic and natural disturbances (as a result of climatic changes) to the C pools include fire, crop harvest,
111 changes to the Gross Primary Productivity (GPP), litterfall, autotrophic and heterotrophic respiration (Krinner et al., 2005;
112 Guimberteau et al., 2018). The C-cycle processes are represented by a C emulator that reproduces for each PFT all C pools
113 and fluxes between the pools exactly as in ORCHIDEE in absence of erosion. A net land use change scheme is included in
114 the emulator with mass-conservative bookkeeping of SOC and C input when a PFT is changed into another from
115 anthropogenic land use change (Naipal et al., 2018). The sediment budget model has been added in the emulator to
116 simulate large-scale long-term soil and SOC redistribution by water erosion using coarse-resolution precipitation,
117 land-cover and LAI data from Earth System Models (Naipal et al. 2015, 2016). The C emulator including erosion removal
118 was developed by Naipal et al. (2018) to reproduce the SOC vertical profile, removal of soil and SOC starting from the
119 topsoil, and compensatory SOC storage from litter input. As soil erosion is assumed not to change soil and hydraulic
120 parameters but only the SOC dynamics, the emulator allows substituting for the ORCHIDEE model and performing
121 simulations on time scales of millennia with a daily time step, which would be a very computationally expensive or nearly
122 impossible with the full LSM. The concept and all equations of the emulator are described in Naipal et al. (2018). The
123 following subsections describe the different components of the CE-DYNAM that couples the C and soil removal scheme
124 (Naipal et al., 2018) with the horizontal transport and burial of eroded soil and C (Naipal et al., 2016).

125

126 **2.2 The soil erosion scheme**

127

128 The potential gross soil erosion rates are calculated by the Adjusted Revised Universal Soil Loss Equation (Adj. RUSLE)
129 model (Naipal et al., 2015), which is based on the Revised Universal Soil Loss Equation (RUSLE) (Renard et al., 1997)
130 and part of the sediment budget model (Naipal et al., 2016) (Fig 1). In the Adj. RUSLE the yearly average soil erosion rate
131 is a product of rainfall erosivity (R), slope steepness (S), land cover and management (C_m) and soil erodibility (K):

132

$$133 \quad E = S \times R \times K \times C_m \quad (1)$$

134

135 Note that the original RUSLE model further includes a slope-length factor (L), which gives the length of a field in the
136 direction of steepest descent, and a support practice factor (P), which accounts for management practices to mitigate soil
137 erosion. These two factors have been excluded here, because their quantification still includes many uncertainties and is
138 not practical for applications at regional to global scales. These factors are largely affected by local man-made structures

139 (such as field size) and management practices, which are difficult to assess for present day and whose changes over the past
140 are even more uncertain. In addition, we focus in this study on the potential effect of soil erosion on the C budget without
141 erosion-control (EC) practices.

142
143 Naipal et al. (2015) have developed a methodology to derive the *S* and *R* factors from 5 arcmin resolution (5 x 5 arcminute
144 raster) data on elevation and precipitation, hereby preserving the high-resolution spatial variability in slope and temporal
145 variability in erosivity. In the rest of the manuscript we will refer to *X* by *X* km/arcminute raster cells always with *X*
146 km/arcmin resolution. Despite the comparatively coarse resolution of the erosion model, the so derived *R* factor was shown
147 to compare well with the corresponding high-resolution product published by Panagos et al. (2017). In the study of Naipal
148 et al. (2016), where the soil erosion model was applied for the last millennium, the change in climate was taken into
149 account in the calculation of the *R* factor. For this study, we assume that the climate zones as defined by the
150 Koeppen-Geiger climate classification have not changed drastically since 1850 AD.

151

152 **2.3 The sediment deposition and transport scheme**

153

154 The sediment deposition and transport scheme is adapted from the sediment budget model described by Naipal et al.
155 (2016), which was calibrated and validated for the Rhine catchment (Fig 1). In the sediment budget model rivers and
156 streams are not explicitly simulated. Instead each grid cell contains a floodplain fraction to ensure sediment transport
157 between the grid cells (transport from one grid cell to another can only follow the connectivity of floodplains). It should be
158 noted that global soil databases do not identify floodplain soil as a separate soil class, although national soil databases
159 might. Because we aim to present a carbon erosion model that should be also applicable for other similar catchments, we
160 followed a two-step methodology to derive floodplains in the Rhine catchment. For this purpose we used hydrological
161 parameters and existing data on hillslopes and valleys. First, grid cells were identified that consisted entirely out of
162 floodplains. For this we used the gridded global data set of soil at 5 arcminute resolution, with intact regolith, and
163 sedimentary deposit thicknesses of Pelletier et al. (2016) (Table 1), and identified lowlands and hillslopes based on soil
164 thickness and depth to bedrock. The lowlands were classified as grid cells that contain only floodplains and no hillslopes.
165 Second, we calculated the floodplain fraction (A_{fl}) of a grid cell *i* that has both hillslopes and floodplains as a function of
166 stream length and width based on the methodology developed by Hoffmann et al. (2007):

167

$$168 \quad A_{fl}(i) = L_{stream}(i) \times W_{stream}(i) \quad (2)$$

169

170 Where, L_{stream} is the stream length derived from the HydroSHEDS database (Lehner and Grill, 2013) (Table 1).

171

$$172 \quad W_{stream}(i) = a \times A_{upstream}^b(i) \quad (3)$$

173

174 Where, $A_{upstream}$ is the upstream catchment area, and a is equal to 60.8, and b is equal to 0.3.

175
176 The parameters a and b have been derived using the scaling behavior of floodplain width as estimated from measurements
177 on the Rhine (Hoffmann et al., 2007). The sediment deposition on hillslopes (D_{hs}) and floodplains (D_f) is calculated as a
178 function of the gross soil removal rates (E) according to Naipal et al. (2016) with the following equations:

179
180
$$D_f(i) = f(i) \times E(i) \quad (4a)$$

181
182
$$D_{hs}(i) = (1 - f(i)) \times E(i) \quad (4b)$$

183
184
$$f(i) = a_f \times e^{\left(\frac{b_f \times \theta(i)}{\theta_{max}}\right)} \quad (5)$$

185
186 Where, f is the floodplain deposition factor at 8 km resolution that determines the fraction of eroded material transported
187 and deposited in the floodplain fraction of a grid cell. a_f and b_f are constants that relate f to the average topographical slope
188 (θ) of a grid cell depending on the type of land cover. θ_{max} is the maximum topographical slope of the entire Rhine
189 catchment.

190
191 The parameters a_f and b_f are chosen in such a way that f varies between 0.2 and 0.5 for cropland, reflecting the decreased
192 sediment connectivity between hillslopes and floodplains created by man made structures such as ditches and hedges. For
193 natural vegetation such as forests and natural grassland, a_f and b_f are chosen in a way that f varies between 0.5 and 0.8
194 assuming that in these landscapes hillslopes and floodplains are well-connected. This assumption on the reduced sediment
195 connectivity for agricultural landscapes is supported by several previous studies on the effect of erosion on sediment yield
196 (Hoffmann et al., 2013a; de Moor and Verstraeten, 2008; Gumiere et al., 2011; Wang et al., 2015). These studies showed
197 that man-made activities on agricultural landscapes result in a trapping of eroded soil in colluvial deposition sites, reducing
198 the sediment transport from hillslopes to floodplains. The model parameter f has been calibrated for the Rhine catchment
199 by Naipal et al. (2016), where the ranges mentioned above are found to produce a ratio between hillslope and floodplain
200 sediment storage that was comparable to observations. The studies of Wang et al. (2010; 2015) identified a range for the
201 hillslope sediment delivery to be between 50 and 80 %, which is similar to the range in the (1-f) factor in our model. In
202 each case and within the defined boundaries, the slope gradient determines the final value of f . Eroded material that has not
203 been deposited in the floodplains stays on the hillslopes and is assumed to be deposited at the foot of the hillslopes as
204 colluvial sediment.

205
206 The floodplain fractions of the grid cells are connected through an 8 km resolution flow routing network (Naipal et al.,
207 2016), where the rivers and streams are indirectly included in the floodplain area but not explicitly simulated. By routing
208 the sediment and C through the floodplain fractions of grid cells we lump together the slow process of riverbank erosion by

209 river dynamics (time scale \approx a few years to thousands of years), and the rather fast process of transport of eroded material
 210 by the rivers (time scale \approx days). The rate by which sediment and SOC leave the floodplain of a grid cell to go to the
 211 floodplain of an adjacent grid cell is determined by the sediment residence time. The sediment residence time (τ) is a
 212 function of the upstream contributing area ($Flowacc$):

$$213 \tau(i) = e^{\frac{Flowacc(i)-a_{\tau}}{b_{\tau}}} \quad (6)$$

214
 215 The study of Hoffmann et al. (2008) showed that the majority of floodplain sediments have a residence time that ranges
 216 between 0 and 2000 years, with a median of 50 years. The constants a_{τ} and b_{τ} are chosen in such a way that basin τ varies
 217 between the 5th and 95th percentile of those observations, with a median for the whole catchment of 50 years. These
 218 constants are uniform for the whole basin. These constants need to be calibrated based on local data of sediment ages
 219 before CE-DYNAM can be applied to other catchments.

220
 221 Floodplain C storage follows the same residence time as sediment on top of the actual decomposition rate of C in a grid
 222 cell of ORCHIDEE. The routing of sediment and C between the grid cells follows a multiple-flow routing scheme. In this
 223 scheme the flow coming from a certain grid cell is distributed across all lower-lying neighbors based on a weight (W ,
 224 dimensionless) that is calculated as a function of the contour length (c):

$$225 W_{(i+k,j+l)} = \frac{\theta_{(i+k,j+l)} \times c_{(i+k,j+l)}}{\sum_{k,l=-1}^{k,l=1} [\theta_{(i+k,j+l)} \times c_{(i+k,j+l)}]} \quad (7)$$

226
 227 Where c is $0.5 \times \text{grid size}$ (m) in the cardinal direction and $0.354 \times \text{grid size}$ (m) in the diagonal direction. (i, j) is the grid cell
 228 in consideration where i counts grid cells in the latitude direction and j in the longitude direction. $i+k$ and $j+l$ specify the
 229 neighboring grid cell where k and l can be either -1, 0 or 1. θ is calculated as the division between the difference in
 230 elevation (h) give in meters difference and the grid cell size (d), also in meters:

$$231 \theta_{(i+k,j+l)} = \frac{h_{(i,j)} - h_{(i+k,j+l)}}{d} \quad (8)$$

232
 233 The sediment and C routing is done continuously at a daily time-step to preserve the numerical stability of the model. More
 234 detailed explanation of the methods presented in this section can be found in the study of Naipal et al. (2016).

235 2.4 Litter dynamics

236
 237 The four litter pools in the emulator are an below- and an above- ground litter pool, each split into a metabolic and
 238 structural pool with different turnover rates as implemented in ORCHIDEE (Krinner et al., 2005). The belowground litter

243 pools consist mostly out of root residues. Both the biomass and litter pools have a loss flux due to fire as incorporated in
244 ORCHIDEE by the Spitfire model of Thonicke et al. (2010). The litter that is not respired or burnt is transferred to the SOC
245 pools based on the Century model (Parton et al., 1987), which was modified by Naipal et al. (2018) to include a vertical
246 discretization scheme for SOC.

247
248 The vertical discretization scheme was introduced in the emulator to account for a declining C input and SOC respiration
249 with depth, and consists of 20 soil layers with each 10 cm thickness. The litter to soil fluxes from aboveground litter pools
250 are all attributed to the top 10 cm of the soil profile. The litter to soil fluxes from belowground litter pools are distributed
251 exponentially over the whole soil profile according to:

$$252 \quad I_{be}(z) = I_{0be} \times e^{-r \times z} \quad (9)$$

253
254 Where I_{0be} is the below-ground litter input to the surface soil layer and r is the PFT-specific vertical root-density attenuation
255 coefficient as used in ORCHIDEE. The sum of all layer-dependent litter to soil fractions is equal to the total litter to soil
256 flux as calculated by ORCHIDEE. The vertical SOC profile is modified by erosion and the resulting deposition fluxes,
257 which is discussed in detail in the following sections.

258

259 **2.5 Crop harvest and yield**

260

261
262 We adjusted the representation of crop harvest from ORCHIDEE by assuming a variable harvest index for C3 plants that
263 increases during the historical period as shown in the study of Hay (1995) for wheat and barley, which are also the main C3
264 crops in the Rhine catchment. The harvest index is defined by the ratio of harvested grain biomass to above-ground dry
265 matter production (Krunner et al., 2005). In this study the harvest index increases linearly between 0.26 and 0.46 (Naipal et
266 al. 2018) consistent with the average values of Hay (1995). We also found that in certain cases the cropland Net Primary
267 Productivity (NPP) was too high during the entire period of 1850-2005, especially in the early part of the 20th Century. This
268 is because the cropland photosynthetic rates were adjusted in ORCHIDEE to give a cropland NPP representative of present
269 day values that are higher than for the low input agriculture of the early 20th Century. To derive a more realistic NPP for
270 crop and barley in the Rhine catchment we used the long-term crop yield data obtained from a dataset on 120000 yield
271 observations over the 20th century in Northeast French Départements (NUTS3 administrative division) (Schauberger et al.,
272 2018). According to the yield data assembled by Schauberger et al. (2018), yields in Northeast France (covers part of the
273 Rhine catchment) for these crops increased fourfold during the last century. Note that crop residues like straw constituted a
274 larger fraction of the total biomass in 1850 than in 2005, but those residues were likely collected and used for animal feed,
275 housing fuel. We did not account for this harvest of residue in the simulation of SOC.

276

277 2.6 SOC dynamics without erosion

278

279 The change in the C content of the PFT-specific SOC pools in the emulator without soil erosion was described by Naipal et
280 al. (2018) (Fig 1) as follows:

281

$$282 \frac{dSOC_a(t)}{dt} = lit_a(t) + k_{pa} \times SOC_p(t) + k_{sa} \times SOC_s(t) - (k_{ap} + k_{as} + k_{0a}) \times SOC_a(t) \quad (10)$$

283

$$284 \frac{dSOC_s(t)}{dt} = lit_s(t) + k_{as} \times SOC_a(t) - (k_{sa} + k_{sp} + k_{0s}) \times SOC_s(t) \quad (11)$$

285

$$286 \frac{dSOC_p(t)}{dt} = k_{ap} \times SOC_a(t) + k_{sp} \times SOC_s(t) - (k_{pa} + k_{0p}) \times SOC_p(t) \quad (12)$$

287

288 Where, SOC_a , SOC_s , and SOC_p (g C m^{-2}) are the active, slow and passive SOC, respectively. The distinction of these SOC
289 pools, defined by their residence times, are based on the study of Parton *et al.* (1987). The active SOC pool has the lowest
290 residence time (1 - 5 years) and the passive the highest (200-1500 years). lit_a and lit_s ($\text{g C m}^{-2} \text{ day}^{-1}$) are the daily litter
291 input rates to the active and slow SOC pools, respectively; k_{0a} , k_{0s} and k_{0p} (day^{-1}) are the respiration rates of the active,
292 slow and passive pools, respectively; k_{as} , k_{ap} , k_{pa} , k_{sa} , k_{sp} are the coefficients determining the flux from the active to the
293 slow pool, from the active to the passive pool, from the passive to the active pool, from the slow to the active pool and
294 from the slow to the passive pool, respectively.

295

296 The vertical C discretization scheme in the emulator assumes that the SOC respiration rates decrease exponentially with
297 depth:

298

$$299 k_i(z) = k_{0i}(z) \times e^{-re \cdot z} \quad (13)$$

300

301 Where k_i is the respiration rate at a soil depth z and re (m^{-1}) is a coefficient representing the impact of external factors, such
302 as oxygen availability that decreases with depth. k_0 is the respiration rate of the surface soil layer for a certain SOC pool i .
303 The variable re is determined in such a way that the total soil respiration of a certain pool over the entire soil profile
304 without erosion is similar to the output of the full ORCHIDEE model. Detailed description of how this is done can be
305 found in the study of Naipal et al. (2018).

306

307 2.7 Net C erosion on hillslopes

308

309 In the model we assume that soil erosion takes place on hillslopes, and not in the floodplains due to the usually low
310 topographical slope of floodplains. The factor $(1-f)$ determines the fraction of the eroded soil that is deposited in the
311 colluvial reservoirs (Fig 1). Soil erosion always removes a fraction of the SOC stock in the upper soil layer depending on

312 the erosion rate and bulk density of the soil. The next soil layer contains less C and therefore at the following time-step less
 313 C will be eroded under the same erosion rate. To account for this effect, the SOC profile evolution is dynamically tracked
 314 in the model and updated at a daily time step, conform with the method of Wang et al. (2015). First, a fraction of the C
 315 from each soil pool in proportion to the erosion height is removed from the surface layer. Then, at the same erosion rate,
 316 SOC from the subsoil layer becomes the surface layer, maintaining the soil layer thickness in the vertical discretization
 317 scheme. Similarly, the SOC from the subsoil later also moves upward one layer. The removal of C by erosion also triggers
 318 a compensatory C sink due to the reduction in SOC respiration on eroding land. This compensatory C sink and reduced C
 319 erosion over time will ultimately lead to an equilibrium state. The change in C content due to net erosion (the eroded
 320 sediment/C that leaves the hillslopes after deposition) of the PFT-specific pools for hillslopes can be represented by the
 321 following equations:

$$322 \quad \frac{dSOC_{HSi}(z,t)}{dt} = k_E \times SOC_{HSi}(z+1,t) - k_E \times SOC_{HSi}(z,t) \quad (14)$$

323
 324
 325 Where $dSOC_{HSi}(z,t)$ is the change in hillslope SOC of a component pool i at a depth z and at time step t . The daily net
 326 erosion fraction k_E (dimensionless) is calculated as following:

$$327 \quad k_E = \frac{f \times \left(\frac{E}{365}\right)}{BD \times dz} \times EF \quad (15)$$

328
 329
 330 Where, E is the gross soil erosion rate ($t \text{ ha}^2 \text{ year}^{-1}$), f is the floodplain deposition factor, BD is the average bulk density of
 331 the soil profile ($g \text{ cm}^{-3}$), dz is the soil thickness ($=0.1 \text{ m}$), and EF is the C enrichment factor that is set to 1 by default. A
 332 model sensitivity analysis will be performed (see section 4.3) with $EF > 1$ to represent a higher C concentration in eroded
 333 soil compared to the original soil as a result of the selectivity of erosion.

334
 335 Hillslope erosion without the deposition term has already been tested and applied at the global scale as part of the C
 336 removal model presented by Naipal et al. (2018).

337 338 **2.8 C deposition and transport in floodplains**

339
 340 The SOC-profile dynamics of floodplains are controlled by: (1) C input from the hillslopes, (2) C import by lateral
 341 transport from the floodplain fractions of upstream grid cells, and (3) C export to the floodplain fractions of downstream g
 342 grid cells (Fig 1). First, the net erosion flux from the surface layer of the hillslope fraction of the grid cell ($k_E \times SOC_{HS}$
 343 ($z=0$)) is incorporated in the surface layer of the floodplain. At the same deposition rate, the SOC of the surface layer of the
 344 floodplain is incorporated in the subsoil layer. Similarly, a fraction of the SOC of the subsoil layer is moved downward one
 345 layer. We will refer to this process as the ‘downward’ moving of C in the soil layer profile. It should be noted that C
 346 selectivity during transport and deposition is not taken into account here, meaning that the C pools of the deposited

347 material are the same as the eroded material from the topsoil of eroding areas. At the same time a fraction of the C of the
 348 surface layer proportional to the sediment residence time (τ) is exported out of the catchment following the sediment
 349 routing scheme, resulting in the ‘upward’ moving of the C from the subsoil layers. This process represents the river bank
 350 erosion and resulting POC export by the water network, although rivers and streams are not explicitly represented in the
 351 model. As we do not have information on the sub-grid spatial distribution of land cover fractions we first sum the exported
 352 C flux over all PFTs before assigning the flux proportionally to the land cover fractions of the receiving
 353 downstream-located grid cells. The C that is imported from the neighboring grid cells follows the same procedure as the
 354 deposition of eroded material, and results in a ‘downward’ moving of the C in the soil profile. The change in C content due
 355 to deposition and routing of the PFT-specific SOC pools for floodplains can be represented by the following equations:
 356

$$357 \frac{dSOC_{FLi}(z,t)}{dt} = \left((k_D + k_{i_{out}}) \times SOC_{FLi}(z-1, t) \right) + \left(\frac{1}{(\tau \times 365)} \times SOC_{FLi}(z+1, t) \right) - \left(\left(k_D + \frac{1}{(\tau \times 365)} + k_{i_{out}} \right) \times SOC_{FLi}(z, t) \right),$$

358 for $z > 0$ (16)

$$360 \frac{dSOC_{FLi}(0,t)}{dt} = \sum_{n=1}^{n=9} \left(k_{i_{out}}(n) \times SOC_{FLi}(0, t)(n) \right) + (k_E \times SOC_{HSi}(0, t)) + \left(\frac{1}{(\tau \times 365)} \times SOC_{FLi}(1, t) \right) - \left(\left(k_D + \frac{1}{(\tau \times 365)} + k_{i_{out}} \right) \times SOC_{FLi}(0, t) \right)$$

361 , for $z=0$ (17)

362
 363 Where n is the neighboring grid cell that flows into the current grid cell, $dSOC_{FLi}(z,t)$ is the change in floodplain SOC of a
 364 component pool i at a depth z and at time step t , and SOC_{HS} is the hillslope SOC stock. k_D is the deposition rate and equal
 365 to:

$$367 k_D = \frac{k_E \times AREA_{HS}}{AREA_{FL}} \quad (18)$$

368
 369 Where $AREA_{HS}$ is the hillslope area and $AREA_{FL}$ is the floodplain area (m^2). $k_{i_{out}}$ is the import rate per C pool i from
 370 neighboring grid cells (dimensionless) and can be calculated as:

$$372 k_{i_{out}} = \frac{\sum_{n=1}^{n=9} (W \times \frac{1}{\tau \times 365} \times AREA_{FL})(n)}{AREA_{FL}} \quad (19)$$

373
 374 Where, W is the weight index of equation 7.

375
 376 The first term of equation 16 represents the ‘downward’ moving of the incoming C related to the C deposition flux from
 377 the hillslope fraction of the grid cell and the lateral C import flux from the floodplain fractions of upstream neighboring
 378 grid cells. The second term represents the ‘upward’ moving of SOC related to the lateral C transfer to downstream
 379 neighboring grid cells. The third term of equation 16 represents the total C loss flux from the current soil layer z , which is a

380 result of either the ‘upward’ or ‘downward’ moving of the C in the soil profile. The first term of equation 17 represents the
381 incoming lateral C flux from the floodplains of the upstream neighboring grid cells. The second term represent the C
382 deposition flux coming from the hillslope fraction of the grid cell. The third term represents the ‘upward’ moving of the
383 SOC from the subsoil layer to the topsoil layer as a result of sediment/C routing. The last term of equation 17 represents
384 the total loss of C from the topsoil layer, of which part is distributed across the neighboring grid cells downstream ($\frac{1}{(\tau \times 365)}$
385), and part is moved ‘downwards’ in the soil profile as a result of C deposition (k_D) and the incoming later C from upstream
386 grid cells (k_{out}).

387

388 **2.9 The land use change bookkeeping model**

389

390 The land use change bookkeeping scheme includes the yearly changes in forest, grassland and cropland areas in each grid
391 cell as reconstructed by Peng et al. (2017) (Table 1). Peng et al. (2017) derived historical changes in PFT fractions based on
392 LUHv2 land use dataset (Hurtt et al., 2011), historical forest area data from Houghton, and present day forest area from
393 ESA CCI satellite land cover (European Space Agency, ESA, 2014). By using different transition rules and independent
394 forest data to constrain the changes in crop and urban PFTs they derived the most suitable historical PFT maps.

395

396 When land use change takes place, the litter and SOC pools of all shrinking PFTs are summed and allocated proportionally
397 to the expanding PFTs, maintaining the mass-balance. In this way the litter pools and SOC stocks get impacted by different
398 input and respiration rates for each soil layer. When forest is reduced, three wood products with decay rates of 1, 10 and
399 100 years are formed and harvested. The biomass pools of other shrinking land cover types are transformed to litter and
400 allocated to the expanding PFTs. More details on the land use scheme are described in the study of Naipal et al. (2018).

401

402 **2.10 Study-Area**

403

404 The model is tested for the Rhine catchment (Fig 2), which has a total basin area of about 185,000 km² covering five
405 different countries in Central Europe. Its large size is beneficial for the application of a coarse-resolution model such as
406 CE-DYNAM to study large-scale regional dynamics in the C cycle due to soil erosion. The Rhine catchment has a
407 contrasting topography, with steep slopes larger than 20% upstream in the Alps, and large, wide and flat floodplains at the
408 foot of the Alps, the upper Rhine and the lower Rhine. The floodplains store large amounts of sediment and C that originate
409 from eroding hillslopes upstream. These sediment storages provide the possibility to study the long-term effect of erosion
410 on hillslope and floodplain dynamics. Furthermore, the Rhine catchment has been experiencing different stages of land use
411 change over the Holocene, with land degradation dating back to more than 5500 years ago (Dotterweich, 2013). In contrast,
412 during the last two decades there has been a general afforestation and soil erosion has been decreasing. These land use
413 changes and changes in erosion make an interesting and important case to study the effect of anthropogenic activities on
414 the C cycle in Europe.

415

416 In addition, the Rhine catchment has been the focus of many erosion studies providing observations on erosion and
417 sediment dynamics that can be used for model validation (Asselman, 1999; Asselman et al., 2003; Erkens, 2009; Hoffmann
418 et al., 2007, 2008, 2013a, 2013b; Naipal et al., 2016). The global sediment budget model that forms the basis for the
419 sediment dynamics scheme of CE-DYNAM has been validated and calibrated for the Rhine catchment with observations
420 on sediment storage from Hoffmann et al. (2013a) and the derived scaling relationships between sediment storage and
421 basin area (Naipal et al., 2016). Hoffmann et al. (2008, 2013a) did an inventory of 41 hillslope and 36 floodplain sediment
422 and SOC deposits related to soil erosion over the last 7500 years. The floodplain sediment observations consist mostly out
423 of organic material (gyttja, peat) and fine sediments (fine sand, loam, silt) in overbank deposits (Hoffmann et al., 2008).
424 These fine sediments are a result of long-term soil erosion on the hillslopes. Hoffmann et al. (2013a) found that the
425 sediment and SOC deposits were quantitatively related to the basin size according to certain scaling functions, where
426 floodplain deposits increased in a non-linear way with basin size while the hillslope deposits showed a linear increase with
427 basin size. We use these relationships to validate the spatial variability in SOC storage of floodplains and hillslopes
428 simulated by CE-DYNAM. The scaling relationships have the form of a simple power law:

429

$$430 \quad M = a \times \left(\frac{A}{A_{ref}}\right)^b \quad (20)$$

431

432 Where M is the sediment storage or the SOC storage, a is the storage (Mt) related to an arbitrary chosen area A_{ref} , while b is
433 the scaling exponent.

434

435 **2.11 Input data and model simulations**

436

437 To create the C emulator that forms the underlying C cycle part of CE-DYNAM, we first ran the full ORCHIDEE model
438 for the period 1850-2005 at a coarse resolution of 2.5°degrees latitude and 3.75° degrees longitude, and output all C pools
439 and fluxes. The pools and fluxes were then archived together and used to derive the turnover rates to build the emulator.
440 The SOC scheme of the emulator that has been modified to account for soil erosion processes has been made to run at a
441 spatial resolution of 5 arcmin, similar to the original global sediment budget model. Then, we performed three main
442 simulations with CE-DYNAM for the Rhine catchment. Simulation S0: The baseline simulation or no-erosion simulation,
443 where SOC dynamics are similar to the full ORCHIDEE model. Simulation S1: The erosion -only simulation, where the
444 hillslopes erode and all eroded C is respired to the atmosphere without reaching the colluvial and alluvial deposition sites.
445 Simulation S2: The simulation with full sediment dynamics where hillslopes and floodplains are connected and can store or
446 lose C. We ran the emulator for 3000 years at a daily time step with the initial climate and land cover of the period
447 1850-1860. To speed up the spin-up simulations we calculated the temporary equilibrium state of the floodplain SOC pools
448 every 10 years analytically. At the end of the spin-up period the floodplain SOC pools were close to equilibrium, with a
449 yearly change of less than 0.001% of the total floodplain SOC stock. Afterwards, we performed the transient simulations

450 for the period 1851-2005 at a daily time step with changing climate and land cover conditions, using the equilibrium SOC
451 stocks as baseline. To ensure a faster performance of CE-DYNAM we delineated the Rhine catchment in seven large
452 sub-basins and ran the model in parallel for each of the sub-basins at a daily timestep. After each year the sub-basins
453 exchanged the lateral C fluxes with each other.

454
455 We also performed seven additional sensitivity simulations and four additional uncertainty simulations. Simulation S1_EF
456 and S2_EF are performed to test the model assumption of C enrichment during erosion. Here, we changed the enrichment
457 factor EF to two, based on the study of Lugato et al. (2018). Simulations S2_Tmin and S2_Tmax are performed to test the
458 rate of C transport between floodplains. Here we modified the mean sediment residence time for the Rhine catchment to a
459 minimum of 60 years (50 % lower than the current value), and to a maximum of 128 years (50 % higher than the current
460 value), respectively. However, we kept the maximum sediment residence time at 1500 years. Simulations S0_RM, S1_RM
461 and S2_RM are performed to test the model assumption on crop residue management, where we assumed that all
462 above-ground crop litter is harvested.

463
464 For the uncertainty analysis we performed simulations S1_min and S2_min based on a minimum soil erosion scenario, and
465 S1_max and S2_max based a maximum soil erosion scenario. These soil erosion scenarios are derived from the uncertainty
466 ranges in the rainfall erosivity and land cover factors of the erosion model. All the model simulations are summarized in
467 table 2.

468
469 **2.12 Validation methods and data**

470
471 We performed a detailed model validation of the sediment and the C parts of the model according to the following steps:
472 (1) validation of soil erosion rates using observational and high-resolution model estimates for Germany and Europe, (2)
473 validation of C erosion rates using high-resolution model estimates for Europe from Lugato et al. (2018), (3) validation of
474 the spatial variability of hillslope and floodplain C storage using observational results from Hoffmann et al. (2013a), (4)
475 validation of SOC stocks using observational data from a global soil database and a European land use survey.

476
477 The validation of the soil erosion module has been done before in the studies of Naipal et al. (2015, 2016). However, we do
478 it again in this study due to different input datasets. In addition, the validation includes soil erosion data from new global
479 soil erosion studies such as Borrelli et al. (2018) and Panagos et al. (2015). For the validation of gross soil erosion rates we
480 used the high-resolution model estimates of Panagos et al. (2015), who applied the RUSLE2015 model at a 100 m
481 resolution at European scale for the year 2010. Similarly to the Adj.RUSLE, RUSLE2015 is also derived from the original
482 RUSLE model. However, in contrast to our model, RUSLE2015 does include the erosion factors *L* and *P*. Furthermore, our
483 model uses more coarsely resolved input datasets (Table 1), for which the equations for the R and S factors have been
484 modified. The extensive validation of the Adj. RUSLE model in this study and previous studies (Naipal et al., 2015, 2016,
485 2018), shows that despite its coarse resolution, it is applicable at large spatial scales. Thus, even though both Adj.RUSLE

486 and RUSLE2015 are derived from the same erosion model, the differences between the models are large, which justifies
487 our model comparison.

488
489 Furthermore, we used independent high-resolution erosion estimates from the study of Cerdan et al. (2010), available at a 1
490 km resolution at European scale, which were based on an extensive database of measured erosion rates under natural
491 rainfall in Europe. For the comparison we aggregated the high-resolution model results of both datasets to the resolution of
492 CE-DYNAM. We also used the potential soil erosion map of the Federal Institute for Geosciences and Natural Resources
493 of Germany (Bug and Stolz, 2014). This map presents the yearly average soil erosion rates at a 250 m resolution on
494 agricultural land derived from a USLE-based approach, with some modifications to the erosion factors and input data.
495 Before validating our model results we aggregated these high-resolution erosion rates to the coarser resolution of our
496 model.

497
498 Validation of our net soil erosion rates is done based on the 100 m resolution net soil erosion rates derived with the
499 WATEM-SEDEM model (Borrelli et al., 2018). WATEM-SEDEM simulates soil removal by water erosion based on the
500 USLE approach, sediment transport and deposition based on the transport capacity. The model has been extensively
501 employed to estimate net fluxes of sediments across hillslopes at catchment- and regional-scales.

502
503 For the validation of C erosion rates, we used the high-resolution model results from Lugato et al. (2018), where they
504 coupled the RUSLE2015 erosion model to the Century biogeochemistry model. These model results were available at a
505 resolution of 1 km, where each grid cell was composed of an erosion and deposition fraction. The C erosion rates provided
506 by Lugato et al. (2018) were multiplied with the erosion fraction of a 1 km grid cell. Then, the C erosion rates were
507 aggregated to the resolution of CE-DYNAM. Lugato et al. (2018) provided an enhanced and a reduced erosion-induced C
508 sink uncertainty scenario, based on different assumptions for C enrichment, burial and C mineralization during transport. In
509 CE-DYNAM the C erosion rates from simulation S1 are multiplied with the hillslope area to get the total C erosion flux of
510 a grid cell. As the study of Lugato et al. (2018) considers only agricultural areas, we considered only the crop fraction of a
511 grid cell. It should be noted that the SOC dynamics scheme of CE-DYNAM, which is derived from ORCHIDEE LSM, is
512 also based on the Century model. However, there are large differences between the Century model used by Lugato et al.
513 (2018) and the C dynamics scheme of ORCHIDEE used in this study. For example, in the Century model the crop
514 productivity is mediated by nitrogen availability, which is not the case in the ORCHIDEE version used for this study. The
515 Century model also includes some management practices such as crop rotations, which are not represented in ORCHIDEE.
516 The Century model runs at a much higher resolution and is calibrated for agricultural land, while ORCHIDEE also
517 simulates forest, grasslands and bare soil. In this way, the final SOC stocks derived with CE-DYNAM are also a result of
518 erosion from other land cover types and land use changes. This is an important feature for land use change, which is not
519 included in the Century model. Furthermore, the ORCHIDEE LSM has been used in many global intercomparisons and
520 extensively evaluated for C budgets (Mueller et al., 2019; Todd-Brown et al., 2013). Finally, ORCHIDEE also includes the
521 last century change in crop production calibrated against data (Guenet et al., 2018).

522
523 For the validation of the spatial variability of the SOC stocks of hillslopes and floodplains we used the scaling relationships
524 between basin area and SOC storage derived by Hoffmann et al. (2013a). The study by Naipal et al. (2016) found that the
525 global sediment budget model is able to reproduce the scaling behaviour of sediment storage. After analyzing the
526 dependence of this scaling behavior, they argue it is an emergent feature of the model and mainly dependent on the
527 underlying topography. This indicates that the scaling features of floodplain and hillslope sediment and C storage should
528 also be applicable to a more recent time period. In order to evaluate the ability of CE-DYNAM to reproduce this scaling
529 behavior, we selected the grid cells that contained the points of observation of the study of Hoffmann et al. (2013a) and
530 performed a regression of the basin area (defined as the upstream contributing area) and the SOC storage for floodplains
531 and hillslopes separately. Comparing the absolute values of the sediment and SOC storages of each grid cell from
532 Hoffmann et al. (2013a) was not possible due to the difference in the time-period of the studies, where Hoffmann et al.
533 (2013a) focussed on the entire Holocene, while our study focussed only on the period from 1850 AD.

534
535 For the validation of the total SOC stocks we used the Global Dataset for Earth System Modeling (GSDE) (Shangguan et
536 al., 2014) available at a spatial resolution of 1 km and the Land Use/Land Cover Area Frame Survey (LUCAS) (Palmieri et
537 al., 2011). The LUCAS topsoil SOC stocks, available at a high spatial resolution of 500 m, were calculated using the
538 LUCAS SOC content for Europe (de Brogniez et al., 2015) and soil bulk density derived from soil texture datasets
539 (Ballabio et al., 2016).

540

541 **3 Results**

542

543 Due to large uncertainties in the model and validation data for the Alpine region we only present and discuss the model and
544 validation results for the non-Alpine part of the Rhine catchment.

545

546 **3.1 Model validation**

547 In this section we present the model validation results using the methods and data described in detail in the previous
548 section.

549

550 We find that the quantile distribution of the simulated gross soil erosion rates compares well to the distributions of other
551 observational and high-resolution modelling studies (Cerdan et al., 2010, Panagos et al., 2015, Bug et al., 2014), although
552 CE-DYNAM usually underestimates the very large soil erosion rates such as is found by Cerdan et al. (2010) (Fig 3A, B,
553 C). This is due to the coarse spatial and temporal resolution of CE-DYNAM, and the lack of the slope-length factor (L)
554 (Cerdan et al. (2010) assumed a constant slope length of a 100m). It should be noted that our study, Cerdan et al. (2010)
555 and Bug et al. (2014) simulated potential soil erosion rates, not accounting for EC practices represented by the P-factor.

556

557 We also find that the quantile distribution of the simulated net soil erosion from hillslopes compares well with the
558 distribution from the high-resolution modelling study of Borrelli et al. (2018) (Fig 3D). In addition we performed a spatial
559 comparison of our simulated gross and net erosion rates to those of the studies mentioned above. For this purpose we
560 delineated 13 sub-basins in the Rhine catchment (Fig S3). Table 3 summarizes the resulting goodness-of-fit statistics of this
561 comparison and shows that our erosion model is generally in good agreement with the other studies at sub-basin level,
562 except for net soil erosion. The estimation of the net soil erosion between our study and the study of Borrelli et al. (2018) is
563 done in different ways, which may explain the difference in the results. In our study the deposition of sediment in hillslopes
564 is explicitly calculated as a function of the slope, and vegetation type/cover. Borrelli et al. (2018) used the transport
565 capacity concept (Van Rompaey et al., 2001). Both methods have their uncertainties when applied at large spatial scales.
566 The method in our study has been designed and calibrated to be used at a large spatial scale, and at coarse resolution, while
567 the method of Borrelli et al. (2018) was originally designed to be applied at spatial scales <100m.

568
569 We find that the quantile distributions of our simulated agricultural C erosion and deposition rates are similar to those of
570 the high-resolution modelling study of Lugato et al. (2018) (Figs 4A-D). Also the spatial variability of the C erosion rates
571 at sub-basin level is in good comparison to the validation data (Table 4). However, the linear regression between soil
572 erosion and C erosion rates of our study lies at the lower end of the relationships derived from the enhanced and reduced
573 erosion scenarios of Lugato et al. (2018) (Fig 5). On the one hand, our study does not include EC practices, leading to
574 substantially larger simulated soil erosion rates in regions with EC. Figure 5 shows that our simulated erosion rates are in
575 general larger than the erosion rates from Lugato et al. (2018), which may be explained by this mechanism. On the other
576 hand, the C erosion rates of our study are lower than those of Lugato et al. (2018), due to the coarse spatial resolution of
577 our underlying C-scheme derived from the ORCHIDEE LSM. The decreased spread in our simulated values is also a result
578 of the coarse resolution of our model.

579
580 Accounting for erosion, deposition and transport of SOC leads to a better representation of the simulated topsoil C stocks
581 per land cover type when compared to SOC stocks of the LUCAS database (Fig 6). The simulated SOC stocks of the top
582 20 cm of the soil profile fall within the quantile range of the LUCAS SOC stocks for cropland and forest (Fig 6). Although
583 the topsoil SOC stocks for grassland improved, a large uncertainty range remains. Furthermore, we find that in both the
584 erosion and no-erosion simulation the SOC stocks for grassland are higher than for forest. This is also observed in the
585 study of Wiesmeier et al. (2012), where they found considerable higher SOC stocks for grassland with a median of 11.8 kg
586 C m⁻² compared to forest based on the analysis of 1460 soil profiles in South-Germany. Furthermore, the comparison of the
587 simulated total SOC stocks to those of the LUCAS and GSDE databases at sub-basin level shows a good model
588 performance with respect to the spatial variability in topsoil SOC stocks (Table 5). To validate the spatial variability of
589 floodplain and hillslope SOC stocks separately, we used the scaling relationships found by Hoffmann et al. (2013a) (section
590 2.12). We find a significantly larger exponent for the scaling relationship between the simulated floodplain SOC storage
591 and basin area compared to the simulated hillslope SOC storage, when using the grid cells that contain the points of
592 observation corresponding to the study of Hoffmann et al. (2013a). This result is in line with what Hoffmann et al. (2013a)

593 found and shows that CE-DYNAM can realistically reproduce the spatial variability in SOC stocks between hillslopes and
594 floodplains (Table 6). However, when deriving the scaling relationships at sub-basin level instead of using individual grid
595 cells we do not find a significant difference in scaling between floodplains and hillslopes (Table 6).

596

597 **3.2 Model application**

598

599 We find an average annual soil erosion rate of $1.44 \pm 0.82 \text{ t ha}^{-1} \text{ year}^{-1}$ over the period 1850-2005, which is about half of the
600 average erosion rate simulated for the last millennium (Naipal et al., 2016) and falls within the range of the average erosion
601 rates of the Holocene (Hoffmann et al., 2013). This soil erosion flux mobilized around $66 \pm 28 \text{ Tg}$ of C over the same time
602 period, of which on average 57 % is deposited in colluvial reservoirs, 43% is deposited in alluvial reservoirs, and 0.2% is
603 exported out of the catchment.

604

605 The lower average annual soil erosion rate over the study period compared to the last millennium is a result of the general
606 afforestation in the non-Alpine part of the Rhine catchment that started around 1910 AD according to the data on land
607 cover and land use (Peng et al., 2017; Fig 7B). This land cover data also shows that forest increases by 24 % over the
608 period 1910-2005, mostly as a result of grassland to forest conversion. Cropland decreases by 6 % over the period 1920
609 and 1970, and is relatively stable afterwards. This afforestation leads to a long-term decreasing trend in gross soil and SOC
610 erosion rates on hillslopes (Fig 7C). The temporal variability in the soil and C erosion rates is a result of direct changes in
611 precipitation, such as the temporary increase in erosion rates over the period 1940-1960 (Fig 7A). Furthermore, we find
612 that the temporal variability in C erosion rates follows the soil erosion rates closely, indicating that soil erosion dominates
613 the variations in C erosion over this time-period, while increased SOC stocks due to CO_2 fertilization and afforestation play
614 a secondary role as a slowly varying trend. It should be noted that the correlation between soil and C erosion might be
615 affected by processes not properly captured by the model such as the selectivity of erosion including the enrichment of C in
616 eroded material.

617

618 The cumulative C erosion removal flux of $66 \pm 28 \text{ Tg}$ of C leads to a cumulative net C sink for the whole Rhine region of
619 $216 \pm 23 \text{ Tg C}$ (Fig 7D). This is about 2.1 – 2.7 % of the cumulative NPP and of the same magnitude as the cumulative
620 land C sink of the Rhine without erosion. It should be noted that these are potential fluxes, assuming that the
621 photosynthetic replacement of C is not affected by the degradation of soil due to the removal of nutrients, declining
622 water-holding capacity and other negative changes to the soil structure and texture (processes not covered by our model).
623 The breaking point in figure 7D around 1910 AD is a result of the climate data used as input.

624

625 To better understand the erosion-induced net C flux, we analyze the erosion-induced C exchange with the atmosphere by
626 creating C budgets for the entire Rhine catchment for the period 1850-1860 and for the period 1950-2005 (Figs 8A&B).
627 These C budgets also shed light on changes in the linkage between lateral and vertical C fluxes over time. As we do not

628 explicitly track the movement of eroded C through all reservoirs (for example between eroding hillslopes and colluvial
629 reservoirs), we make use of the changes in SOC stocks and Net Ecosystem Productivity (NEP), which is the difference
630 between NPP and heterotrophic respiration, of the three main simulations (S0, S1, S2) to derive the erosion-induced
631 vertical C fluxes. By subtracting the NEP of hillslopes (NEP_{HS}) of the no-erosion simulation (S0) from the erosion-only
632 simulation (S1), we derive the additional photosynthetic replacement of SOC on eroding sites (Eq. 21):
633

$$634 \quad E_{rep} = NEP_{HS}(S1) - NEP_{HS}(S0) \quad (21)$$

635
636 Where, E_{rep} is the potential dynamic Photosynthetic replacement of C on eroding sites (assuming no feedback of erosion on
637 NPP). Part of the eroded C that is transported to and deposited in colluvial reservoirs can be respired or buried (Eq. 22).
638 The difference between NEP of simulation S2 and S1 is the NEP caused by the deposition of eroded C in colluvial areas
639 and equal to the difference between the burial and respiration of C in colluvial sites. As we do not explicitly track the
640 respiration of deposited material in the model, we can only derive the net respiration or net burial of colluvial deposits
641 ($R_{C_{net}}$) with the following equation:
642

$$643 \quad R_{C_{net}} = NEP_{HS}(S2) - NEP_{HS}(S1) \quad (22)$$

644
645 The same concept can be applied for the net respiration of floodplains:
646

$$647 \quad R_{a_{net}} = NEP_{FL}(S2) - NEP_{FL}(S0) \quad (23)$$

648
649 Where, NEP_{FL} is the floodplain NEP, and $R_{a_{net}}$ is the net respiration or net burial of alluvial deposits. Positive values for
650 $R_{a_{net}}$ or $R_{C_{net}}$ indicate a net burial (respiration S2 < respiration S0/S1) of the deposited material.
651

652 We find that the dynamic replacement of C on eroding sites increased by 17-33% at the end of the period despite
653 decreasing soil erosion rates (Figs 8A& B). This increase in the photosynthetic replacement of C is due to the globally
654 increasing CO_2 concentrations that lead to the CO_2 fertilization effect, amplified by the afforestation trend in the Rhine over
655 this period. Without this fertilization effect, soil erosion and deposition would be likely a weaker C sink or even a C source
656 over the period 1850-2005 (Figs S4A & B). This CO_2 fertilization effect promotes a 100% replacement of the eroded C on
657 hillslopes and even leads to a C sink on hillslopes at the end of the study period (Fig 8B). Furthermore, we find that the
658 yearly average gross C erosion flux from eroding sites decreases by 10 - 34 %, while the yearly deposition fluxes in
659 colluvial and alluvial sites decreases by 20 % and 19 - 47 %, respectively. The decrease in the deposition flux to
660 floodplains is compensated by a better sediment connectivity between hillslopes and floodplains due to afforestation.
661 Forests have less man-made structures that can prevent the erosion fluxes from reaching the floodplains, which is

662 represented by a higher floodplain deposition ' f ' factor in the model. The decrease in the erosion flux also leads to a
663 decreased POC export of the catchment at the end of the study period.

664
665 We also find that both the colluvial and alluvial reservoirs show a net respiration flux throughout the time period (Figs 8A
666 & B). This is consistent with previous studies who found that deposition sites can be areas of increased CO₂ emissions
667 (Billings et al., 2019; Van Oost et al., 2012). However, there is a slight difference in the respiration of deposited C between
668 the start and end of the transient period. The respiration of deposited SOC in colluvial sites increases with time while the
669 respiration of deposited SOC in alluvial sites shows rather a decreasing trend. These changes in SOC respiration of
670 deposited material depends on (1) the amount of deposited material, (2) increasing temperatures over 1850-2005 for the
671 entire catchment, and (3) the constant removal of C-rich topsoil and its deposition in alluvial and colluvial reservoirs,
672 which makes the deposited sediments generally richer in C than soils on erosion-neutral sites, providing more substrate for
673 respiration. The largest increase in total respiration of alluvial and colluvial deposits takes place in hilly regions due to the
674 initial increase in erosion rates resulting in large deposits of C. Overall, we find that the increased respiration of deposited
675 material slightly offsets the increased dynamic C replacement, however, the dynamic C replacement on eroding sites still
676 dominates the erosion-induced C sink.

677 678 **4 Discussion**

679
680 In this section we discuss some of the most important model limitations, uncertainties and assumptions.

681 682 **4.1 Initial conditions and past global changes**

683
684 Initial climate and land cover/use conditions, and the length of the transient period are essential parameters that determine
685 the resulting spatial distribution of soil and C. Landscapes are in a constant transient state due to global changes, such as
686 climate change, land use change, accelerated soil erosion. However, we assumed an equilibrium state so that we can
687 quantify the changes during the transient period. The longer the transient period that covers the essential historical
688 environmental changes, the more accurate are the present-day distribution of SOC stocks, sediment storages, and related
689 fluxes. This is especially true when analyzing the redistribution of soil and C as a result of erosion, deposition and
690 transport, as these soil processes can be very slow. For example, the study of Naipal et al. (2016) showed that by simulating
691 the soil erosion processes for the last millennium a spatial distribution of sediment storages that is similar to observations
692 can be found. In this study we simulated the steady state based on the initial conditions of the period 1850-1860 due to
693 constraints in data availability on precipitation and temperature. By focusing only on the period 1850-2005 we miss the
694 effects of significant land use changes in the past that coincided with times of strong precipitation such as in the 14th and
695 18th century (Bork et al., 2003). These major anthropogenic changes in the last Holocene substantially affected the
696 present-day spatial distribution and size of sediment storage and SOC stocks.

697
698 The absolute value of the SOC storage from the S2 simulations of the non-Alpine region of the Rhine catchment for the
699 year 2005 is in the range of 2.74 - 2.99 Pg of C, which is larger than the 1.7 ± 0.6 Pg of C that Hoffmann et al. (2013a)
700 measured. It should be noted that the ORCHIDEE model (S0 simulation) already overestimates the total SOC stock of the
701 non-Alpine region of the Rhine (2.43 Pg of C), when the initial conditions of the period 1850-1860 are used. Due to the
702 fact that we miss the climate and land use changes before the year 1850, we find that floodplains store less SOC than
703 hillslopes. Although this is in contrast to the findings of Hoffmann et al. (2013a), the difference in SOC stocks between
704 floodplains and hillslopes from the S2 simulations is better than the difference derived from the S0 simulation. We find that
705 floodplains store 1.28 - 1.72 and hillslopes 1.7 - 2 Pg of C when erosion and deposition processes are taken into account,
706 compared to 0.69 Pg of C for floodplains and 2.29 Pg of C for hillslopes when these processes are lacking.
707

708 We also find that floodplains have an overall higher C concentration (12 kg m^{-2}) compared to hillslopes (9 kg m^{-2}) at the
709 end of the transient period (Fig 9A), which is in line with the findings of Hoffmann et al. (2013a) and what can be derived
710 from global soil databases. This is a result of higher SOC concentrations in deeper soil layers of floodplains compared to
711 hillslopes (Figs 9 A&B), as is also shown in the study of Hoffman et al. (2013). To be closer to the observational difference
712 between floodplains and hillslopes we would need to consider the period before 1850, extreme climate events, and a higher
713 plant productivity in floodplains resulting from favorable soil nutrient and hydrological conditions.
714

715 **4.2 Model advantages and limitations**

716

717 Although we parameterized and applied CE-DYNAM for the Rhine catchment, it is intended to be made applicable to
718 other large catchments. CE-DYNAM combines soil erosion processes, for which small scale differences in topography are
719 of utter importance, with a state-of-the-art representation of large-scale SOC dynamics driven by land use and
720 environmental factors (climate, atmospheric CO_2) as simulated by the ORCHIDEE LSM. The flexible structure of
721 CE-DYNAM makes the model adaptable to the SOC dynamics of other LSMs. In this way it is possible to study the main
722 processes behind the linkages between soil erosion and the global C cycle.
723

724 CE-DYNAM explicitly accounts for hillslope and floodplains re-deposition, which is to our knowledge unique for a
725 large-scale C erosion model and highly novel. However, it still lacks important processes affecting the C dynamics in
726 floodplains. The model does not account for a slower respiration rate due to low-oxygen conditions, physical and chemical
727 stabilization (Berhe et al., 2008; Martínez-mena et al., 2019) or a higher NPP for nutrient-rich floodplains (Van Oost et al.,
728 2012; Hoffmann et al., 2013). The oxidation and preservation of C in deposition environments, especially in alluvial
729 reservoirs remain highly uncertain (Billings et al., 2019).
730

731 Due to its simplistic nature and coarse-resolution, CE-DYNAM does not resolve rivers and streams explicitly but assumes
732 that they are included in the floodplain part of the grid cells. As a result, CE-DYNAM does not differentiate between
733 eroded hillslope soil that reaches the water network directly (where the residence time of suspended sediment is in the
734 order of days), and the sediment that is first retained in the floodplains before it reaches the water network due to fluvial
735 erosion (sediment residence time is in the order of a few to thousands of years). CE-DYNAM has been developed and
736 calibrated to simulate long-term changes in sediment and C storage on land and not the short-term variations in sediment
737 and POC fluxes carried by rivers. This limits the application of CE-DYNAM in its current form to accurately quantify
738 sediment and POC fluxes of rivers and streams, and to compare them to observations.

739
740 As a result of the above-mentioned model limitation, CE-DYNAM produces a sediment export flux at the end of the year
741 2005 of about 6472 tonnes per year, which is about two orders of magnitude lower than the estimated suspended sediment
742 flux of about 3.15×10^6 tons year⁻¹ from Asselman et al. (2003) or the 0.75×10^6 tons year⁻¹ simulated by Li et al. (2020).
743 This sediment export rate leads to a yearly sediment bound POC export of about 2×10^8 g C year⁻¹ 2005. This POC flux is
744 also two orders of magnitude lower than the 2.6×10^{10} g C year⁻¹ given by the GlobalNEWS2 model (Mayorga et al., 2010)
745 or the 1.5×10^{11} g C year⁻¹ found by Beusen et al. (2005), which is mainly a result of the underestimated simulated sediment
746 export rate.

747
748 Furthermore, CE-DYNAM does not simulate fluvial erosion as a complex function of the channel geometry, riverbank
749 erodibility and sheer stress (Dröge et al., 1992), due to the lack of data on these parameters at the regional scale, and to
750 keep a balance between model complexity and its computational ability. Also, our model does not resolve erosion of the
751 deposited river sediment by flooding events. This simplified model concept for fluvial erosion contributes to the
752 underestimation of sediment and C export in floodplains. Finally, with the current model setup we do not account for large
753 soil erosion events before 1850 or extreme precipitation events that may have a long-term effect on the sediment export
754 rate of the Rhine.

755
756 Although we underestimate the riverine sediment and POC fluxes, we find that the spatial variability in sediment storage
757 and SOC stocks of the sub-basins are within or close to observational uncertainty ranges (Table 5, 6; Naipal et al., 2016).
758 We also find that the C density in the topsoil layers of floodplain soils located downstream of the Rhine and the C
759 concentration of the POC flux are realistic. We find a C concentration of ~3.3 % in the exported fine sediments. Abril et al.
760 (2005) found a 5.5 % POC mass fraction in suspended sediments for the Rhine. The C density of the topsoil layer of the
761 floodplains in the downstream grid cells in the S2 simulations (S2, S2_min, S2_max) is on average 4.47 kg C m^{-2} , which
762 falls within the range of the average C density of $5.13 \pm 1.3 \text{ kg C m}^{-2}$ measured by Hoffmann et al. (2013a) for floodplain
763 overbank deposits. By comparison, the average C density of the topsoil layers of downstream grid cells in the S0
764 simulation is $12.78 \text{ kg C m}^{-2}$, which is an overestimation. Other model uncertainties that may affect the SOC stocks and
765 POC fluxes include: (1) The absence of increased plant productivity of floodplains, and transformations between POC,
766 DOC and CO₂, and their fate in rivers and streams. Increased plant productivity of floodplains is shown to contribute

767 significantly to the higher SOC stocks of floodplains compared to hillslopes, and to the export of DOC and POC to rivers
768 (Van Oost et al., 2012; Hoffmann et al., 2013a).

769
770 In a future study we aim to improve the sediment and POC export, and account for a higher floodplain plant productivity
771 by using a nutrient-enabled version of the ORCHIDEE LSM (Goll et al., 2017).

772
773 Furthermore, the model does not take into account the full effects of the selectivity of erosion, often expressed as the
774 enrichment ratio, where the C content of eroding soil or the deposited sediment can be different from that of the original
775 soil. The enrichment varies substantially across landscapes, while the importance of erosion selectivity for C is still under
776 debate (Nadeu et al., 2015; Wang et al., 2010). However, we did a simple sensitivity test to study the effect of C enrichment
777 by erosion (section 4.3).

778
779 CE-DYNAM does not account for different ratios between the SOC pools (active, slow, passive) with depth due to the
780 limitation in information to constrain these fractions for floodplains and hillslopes. However, this can be potentially
781 important for respiration of C in depositional sites and during transport. Studies show that the labile C is decomposed first
782 during sediment transport and directly after deposition, leaving behind the more recalcitrant C in deposition sites (Berhe et
783 al., 2007; Billings et al., 2019). Due to the simplistic nature of our coarse-resolution model and the lack of data on
784 oxidation of eroded C during transport we did not include C respiration during transport in the model.

785
786 The current SOC scheme of CE-DYNAM does also not account for different residence times of SOC as a function of
787 landscape position along a hillslope. The SOC decomposition rates can vary significantly along a hillslope due to changes
788 in soil moisture, temperature, aggregation, and the transport of minerals and nutrients (Doetterl et al., 2016). Currently,
789 these processes are not resolved in coarse resolution LSMs, contributing to the uncertainty in the large-scale linkage
790 between soil erosion and SOC dynamics.

791
792 Furthermore, there is no feedback between soil erosion and plant productivity in the model. To account for this feedback,
793 soil erosion processes would need to be explicitly included in a LSM, such as ORCHIDEE, which would increase the
794 computational complexity of the simulations substantially. The lack of this feedback results in an unlimited dynamic
795 replacement of C on eroding sites.

796
797 Currently, the erosion scheme of CE-DYNAM does not include the L (slope-length) and P (support-practice) factors. This
798 might induce some bias in the results, especially for agricultural land. In a future study we aim to make CE-DYNAM better
799 applicable for agricultural land, where these factors play an important role. For this purpose we will focus on the
800 development of new methods that can quantify the L and P factors reliably at the global scale, and will need to re-calibrate
801 the Adj.RUSLE model. Our decision of leaving out the L and P factors from the erosion equation in this study is based on
802 the global study of Doetterl et al. (2012), which showed that the S, R, C and K factors explain approximately 78 % of the

803 total erosion rates on cropland in the USA. This indicates that on cropland the L and P factors, which are related to
804 agriculture and land management, contribute only for 22 % to the overall erosion rates. This percentage is comparable to
805 the uncertainty range in the estimation of the S, R, C and K factors at the regional scale from coarse resolution data. Renard
806 and Ferreira (1993) also mention that the soil loss estimates are less sensitive to slope-length than to most other factors.
807 Furthermore, various studies argue that the estimation of the L factor for large areas is complicated and thus can induce
808 significant uncertainty in soil erosion rates calculated based on coarse resolution data (Foster et al., 2002; Kinnell, 2007).
809 Especially, for natural landscapes, such as forest, the estimation of the L factor is not straightforward as these natural
810 landscapes usually include steep slopes (Elliot, 2004). In order to stay consistent with the estimation of potential soil
811 erosion for all land cover types, we removed the L factor from the equation. The Adj.RUSLE has been already successfully
812 validated at the regional scale, without the L and P factors where the spatial variability of soil erosion rates compares well
813 to other high resolution modeling studies and observational data and the absolute values fall within the uncertainty ranges
814 of those validation data (Naipal et al., 2015; Naipal et al., 2016; Naipal et al., 2018; and this study). Finally, the aim of this
815 study was to develop and validate a C erosion scheme for applications at the global scale, where the estimation of the L and
816 P factors is limited. By showing that the erosion rates from the Adj.RUSLE and CE-DYNAM are within the uncertainty of
817 other data and modelling studies, we assume that it will be applicable for other large catchments in the temperate region.

818
819 Finally, CE-DYNAM considers only the rather ‘slow’ rill and interrill soil erosion processes, and does not take into
820 account severe erosion processes such as gully erosion and landslides, which are bound to extreme precipitation events.
821 The daily timestep of CE-DYNAM and the current setup of the sediment budget module allows only for long-term yearly
822 average changes in erosion and deposition rates and cannot be applied to estimate episodic erosion and deposition events.

823 824 **4.3 Sensitivity analysis**

825
826 We analyzed the effects of the following model assumptions: (1) C enrichment during erosion, (2) the floodplain sediment
827 residence time, and (3) crop residue management.

828
829 To test the C enrichment we increased the EF (Eq. 15) from 1 to 2, assuming a strong enrichment of C during erosion
830 (section 2.11). We find that this enrichment results in a gross C erosion flux that is 1.61 times larger than the flux without
831 enrichment (Table 7). This leads also to a larger dynamic replacement of C on eroding sites in combination with a larger
832 burial in depositional sites, which is in accordance with the study of Lugato et al. (2018). The resulting C sink from the
833 enrichment simulation is 1.25 times larger than the sink under default conditions (Table 7).

834
835 To test the potential effects of a different sediment residence time on the SOC dynamics, we performed a sensitivity study
836 where we changed the basin average sediment residence time to be 50% higher or 50% lower but keeping the maximum
837 sediment residence time at 1500 years (section 2.11). By changing the average sediment residence time and keeping the
838 maximum fixed, the grid cells with the lowest residence times will undergo the largest changes in the residence time and

839 consequently in the floodplain SOC storage and export. The higher the residence time, the longer the deposited soil C will
840 reside in the floodplains, where it can either be respired or buried in deeper soil layers. Therefore, we find that the effects
841 of the sediment residence time on the SOC dynamics are non-linear. Under default conditions we find the highest SOC
842 storage. A 50 % higher average sediment residence time leads to the lowest total SOC storage, with a decrease of 30 %
843 compared to default conditions, while the erosional C sink is reduced by 20 % (Table 7). This could be explained by a
844 higher C decomposition flux for floodplains due to the long residence time of C in deposition areas. Especially in
845 mountainous regions where the soil erosion flux is large and removes a large part of the labile C, a higher sediment
846 residence time will lead to higher C emissions due to decomposition in floodplains. The turnover seems to dominate over
847 the C burial in deeper layers and export. A 50 % lower average sediment residence time also leads to a decrease (of 8 %) in
848 the total SOC storage and a decrease of 6 % in the erosional C sink compared to default conditions (Table 7). Also here,
849 the largest changes are found in mountainous regions where a low sediment residence time leads to a large export of C,
850 which is then deposited in lower lying, more extensive floodplains. Thus, increasing or decreasing the residence time leads
851 to a smaller total SOC storage, resulting from different spatial distributions of this SOC storage. The POC flux under the
852 high sediment residence time scenario is substantially higher than under default conditions (Table 7).

853
854 To test the effects of crop residue management we harvested all above-ground crop residues (section 2.11). We find that the
855 total litter C stock is about 15 % smaller than the default case by the end of the year 2005. This leads to a total change in
856 the transient SOC stocks that is 20 % smaller under no erosion (S0), and 26 % smaller under erosion (S2) (Table 7). Our
857 findings confirm that soil management practices such as residue management have a substantial effect on the SOC
858 dynamics.

859 860 **5 Conclusions**

861
862 We presented a novel spatially-explicit and process-based C erosion dynamics model, CE-DYNAM, which simulates the
863 redistribution of soil and C over land as a result of water erosion and estimates the implications for C budgets at catchment
864 scale. We demonstrated that CE-DYNAM captures the spatial variability in soil erosion, C erosion and SOC stocks of the
865 non-Alpine region of the Rhine catchment when compared to high-resolution estimates and observations. We also showed
866 that the quantile ranges of erosion and deposition rates and C stocks fall within the uncertainty ranges of previous estimates
867 at basin or sub-basin level. Furthermore, we demonstrated the model ability to disentangle vertical C fluxes resulting from
868 the redistribution of C over land and develop C budgets that shed light on the role of erosion in the C cycle. The simple
869 structure of CE-DYNAM and the relative low amount of parameters make it possible to run several simulations to
870 investigate the role of individual processes on the C cycle such as the removal by erosion only, or the role of deposition and
871 transport. Its compatibility with land surface models makes it possible to investigate the long-term and large-scale effect of
872 erosion processes under various global changes such as increasing atmospheric CO₂ concentrations, changes to
873 precipitation and temperature, and land use change.

874

875 The application of CE-DYNAM for the Rhine catchment for the period 1850-2005 AD reveals three key findings:

- 876 ● Soil erosion leads to a cumulative net C sink of 216 ± 23 Tg by the end of the period, which is in the same order of
877 magnitude as the cumulative land C sink of the Rhine without erosion. This C sink is a result of an increasing
878 dynamic replacement of C on eroding sites due to the CO₂ fertilization effect, despite decreasing soil and C
879 erosion rates over the largest part of the catchment. We conclude that it is important to take into account global
880 changes such as climate change in order to better quantify the net effect of erosion on the C cycle.
- 881 ● After performing a sensitivity analysis on key model parameters we find that the C enrichment by erosion, crop
882 residue management and the residence time of floodplain sediment can substantially change the overall values of
883 C fluxes and SOC storages. However, the main findings, such as soil erosion being a net C sink for the Rhine
884 catchment, remain.
- 885 ● Initial climate and land cover conditions and the transient period over which erosion under global changes takes
886 place are essential for determining if soil erosion is a net C sink or source and to what extent.

887

888 Altogether, these results indicate that despite model uncertainties related to the relative coarse spatial resolution, missing or
889 simplified processes, CE-DYNAM represents an important step forwards into integrating soil erosion processes and
890 sediment dynamics in Earth system models. The next step would be to improve CE-DYNAM with respect to riverine
891 sediment and POC export fluxes and management practices.

892

893 **Code and data availability**

894

895 The source code of CE-DYNAM is included as a supplement to this paper. Model data can be accessed from the Zenodo
896 repository under the doi:10.5281/zenodo.2642452 (not published yet). For the other data sets that are listed in Table 1, it is
897 encouraged to contact the first authors of the original references.

898

899 **Author contributions**

900

901 VN built and implemented the mode. YW provided the basic structure for the model. All authors contributed in the
902 interpretation of the results and wrote the paper.

903

904 **Competing interests**

905

906 *The authors declare that they have no conflict of interest.*

907

908 **Acknowledgements**

909

910 Funding was provided by the Laboratory for Sciences of Climate and Environment (LSCE), CEA, CNRS, and UVSQ.
911 Victoria Naipal, Ronny Lauerwald and Philippe Ciais acknowledges support from the VERIFY project that received
912 funding from the European Union's Horizon 2020 research and innovation program under grant agreement No 776810.
913 Bertrand Guenet acknowledges support from the project ERANETMED2-72-209 ASSESS. We also thank Dr. S. Peng for
914 sharing the PFT maps.

915

916 **References**

917

918 **Abril, G. and Borges, A.V.:** Carbon dioxide and methane emissions from estuaries, Greenhouse gas emissions—fluxes and
919 processes, 187-207, Springer, Berlin, Heidelberg, 2005.

920

921 Asselman, N. E. M.: Suspended sediment dynamics in a large drainage basin : the River Rhine , 1450(November 1998),
922 1437–1450, [https://doi.org/10.1002/\(SICI\)1099-1085\(199907\)13:10<1437::AID-HYP821>3.0.CO;2-J](https://doi.org/10.1002/(SICI)1099-1085(199907)13:10<1437::AID-HYP821>3.0.CO;2-J), 1999.

923

924 Asselman, N. E. M., Middelkoop, H. and van Dijk, P. M.: The impact of changes in climate and land use on soil erosion,
925 transport and deposition of suspended sediment in the River Rhine, *Hydrol. Process.*, 17(16), 3225–3244,
926 doi:10.1002/hyp.1384, 2003.

927

928 Ballabio, C., Panagos, P. and Monatanarella, L.: Geoderma Mapping topsoil physical properties at European scale using the
929 LUCAS database, *Geoderma*, 261, 110–123, doi:10.1016/j.geoderma.2015.07.006, 2016.

930

931 Berhe, A. A., Harte, J., Harden, J. W. and Torn, M. S.: The Significance of the Erosion-induced Terrestrial Carbon Sink,
932 *Bioscience*, 57(4), 337, doi:10.1641/B570408, 2007.

933

934 Berhe, A. A., Harden, J. W., Torn, M. S. and Harte, J.: Linking soil organic matter dynamics and erosion-induced terrestrial
935 carbon sequestration at different landform positions, *J. Geophys. Res. Biogeosciences*, 113(4), 1–12,
936 doi:10.1029/2008JG000751, 2008.

937

938 Beusen, A. H. W., Dekkers, A. L. M., Bouwman, A. F., Ludwig, W., & Harrison, J.: Estimation of global river transport of
939 sediments and associated particulate C, N, and P, *Global Biogeochemical Cycles*, 19(4), doi:10.1029/2005GB002453,
940 2005.

941

942 Billings, S. A., Richter, D. D. B., Ziegler, S. E., Prestegard, K. and Wade, A. M.: Distinct Contributions of Eroding and
943 Depositional Profiles to Land-Atmosphere CO₂ Exchange in Two Contrasting Forests, 7(March),
944 doi:10.3389/feart.2019.00036, 2019.

945

946 Bork, H.R. and Lang, A.: Quantification of past soil erosion and land use/land cover changes in Germany, Long term
947 hillslope and fluvial system modelling, 231-239, Springer, Berlin, Heidelberg, 2003.
948

949 Borrelli, P., Van Oost, K., Meusburger, K., Alewell, C., Lugato, E., Panagos, P.: A step towards a holistic assessment of
950 soil degradation in Europe: Coupling on-site erosion with sediment transfer and carbon fluxes, *Environmental Research*,
951 161, 291-298, doi:<https://doi.org/10.1016/j.envres.2017.11.009>, 2018
952

953 de Brogniez, D., Ballabio, C., Stevens, A., Jones, R. J. A., Montanarella, L. and Van Wesemael, B.: A map of the topsoil
954 organic carbon content of Europe generated by a generalized additive model, *Eur. J. Soil Sci.*, 66(January), 121–134,
955 doi:10.1111/ejss.12193, 2015.
956

957 Bug, J., Stolz, W., Stegger, U.: Potentielle Erosionsgefaehrdung der Ackerboeden durch Wasser in Deutschland,
958 Bundesanstalt fuer Geowissenschaften und Rohstoffe, www.bgr.bund.de/Boden, 2014
959

960 Cerdan, O., Govers, G., Le Bissonnais, Y., Van Oost, K., Poesen, J., Saby, N., Gobin, a., Vacca, a., Quinton, J.,
961 Auerswald, K., Klik, a., Kwaad, F. J. P. M., Raclot, D., Ionita, I., Rejman, J., Rouseva, S., Muxart, T., Roxo, M. J. and
962 Dostal, T.: Rates and spatial variations of soil erosion in Europe: A study based on erosion plot data, *Geomorphology*,
963 122(1–2), 167–177, doi:10.1016/j.geomorph.2010.06.011, 2010.
964

965 Ciais, P., Sabine, C., Bala, G., Bopp, L., Brovkin, V., Canadell, J., Chhabra, A., DeFries, R., Galloway, J., Heimann, M.,
966 Jones, C., Quéré, C. Le, Myneni, R. B., Piao, S. and Thornton, P.: Carbon and Other Biogeochemical Cycles, in *Climate
967 Change 2013: The physical science basis. Contribution of working group I to the fifth assessment report of the
968 intergovernmental panel on climate change* [Stocker, T.F., D. Qin, G.-K. Plattner, M. Tignor, S.K. Allen, J. Boschung, A.
969 Nauels, Y. Xia, pp. 465–570, Cambridge University Press, Cambridge, United Kingdom and New York, NY., 2013.
970

971 De Moor, J. J. W., & Verstraeten, G.: Alluvial and colluvial sediment storage in the Geul River catchment (The
972 Netherlands)—combining field and modelling data to construct a Late Holocene sediment budget, *Geomorphology*,
973 95(3-4), 487-503, 2008
974

975 Doetterl, S., Van Oost, K. and Six, J.: Towards constraining the magnitude of global agricultural sediment and soil organic
976 carbon fluxes, *Earth Surf. Process. Landforms*, doi:10.1002/esp.3198, 2012.
977

978 Doetterl, S., Berhe, A. A., Nadeu, E., Wang, Z., Sommer, M., & Fiener, P.: Erosion, deposition and soil carbon: a review of
979 process-level controls, experimental tools and models to address C cycling in dynamic landscapes, *Earth-Science Reviews*,
980 154, 102-122, 2016.
981

982 Dotterweich, M.: Geomorphology The history of human-induced soil erosion : Geomorphic legacies , early descriptions
983 and research , and the development of soil conservation — A global synopsis, *Geomorphology*, 201(November), 1–34,
984 doi:10.1016/j.geomorph.2013.07.021, 2013.

985

986 Dröge, B., Engel, H., & Götz, E.: Channel erosion and erosion monitoring along the Rhine River, *Erosion and Sediment*
987 *Transport Monitoring Programmes in River Basins*, 210, 493-503, 1992.

988

989 Elliot, W. J.: WEPP INTERNET INTERFACES FOR FOREST EROSION PREDICTION 1, *JAWRA Journal of the*
990 *American Water Resources Association*, 40(2), 299-309, 2004.

991

992 Erkens, G.: *Sediment dynamics in the Rhine catchment*, Utrecht University, Faculty of Geosciences, Utrecht., 2009.

993

994 Foster, G. R., Yoder, D. C., Weesies, G. A., McCool, D. K., McGregor, K. C., & Bingner, R. L: *User’s Guide—revised*
995 *universal soil loss equation version 2 (RUSLE 2)*. USDA–Agricultural Research Service, Washington, DC., 2002.

996

997 Frieler, K., Lange, S., Piontek, F., Reyer, C. P. O., Schewe, J., Warszawski, L., Zhao, F., Chini, L., Denvil, S., Emanuel, K.,
998 Geiger, T., Halladay, K., Hurtt, G., Mengel, M., Murakami, D., Ostberg, S., Popp, A. and Riva, R.: Assessing the impacts
999 of 1.5 °C global warming – simulation protocol of the Inter-Sectoral Impact Model Intercomparison Project (ISIMIP2b),
1000 *Geosci. Model Dev.*, 10, 4321–4345, 2017.

1001

1002 Galy, V., Peucker-Ehrenbrink, B., & Eglinton, T. Global carbon export from the terrestrial biosphere controlled by erosion.
1003 *Nature*, 521, 204–207. <https://doi.org/10.1038/nature14400>, 2015.

1004

1005 Guenet, B., Camino-Serrano, M., Ciais, P., Tifafi, M., Maignan, F., Soong, J. L., & Janssens, I. A.: Impact of
1006 priming on global soil carbon stocks, *Global change biology*, 24(5), 1873-1883, 2018.

1007

1008 Gumiere, S. J., Le Bissonnais, Y., Raclot, D., & Cheviron, B.: Vegetated filter effects on sedimentological connectivity of
1009 agricultural catchments in erosion modelling: a review. *Earth Surface Processes and Landforms*, 36(1), 3-19, 2011.

1010

1011 Hay R.K.M.: Harvest index: a review of its use in plant breeding and crop physiology, *Ann. appl. Biol.*, 126, 197–216,
1012 1995.

1013

1014 Hoffmann, T., Erkens, G., Cohen, K. M., Houben, P., Seidel, J. and Dikau, R.: Holocene floodplain sediment storage and
1015 hillslope erosion within the Rhine catchment, *The Holocene*, 17(1), 105–118, doi:10.1177/0959683607073287, 2007.

1016

1017 Hoffmann, T., Lang, a and Dikau, R.: Holocene river activity: analysing 14C-dated fluvial and colluvial sediments from

1018 Germany, *Quat. Sci. Rev.*, 27(21–22), 2031–2040, doi:10.1016/j.quascirev.2008.06.014, 2008.

1019

1020 Hoffmann, T., Schlummer, M., Notebaert, B., Verstraeten, G. and Korup, O.: Carbon burial in soil sediments from
1021 Holocene agricultural erosion, Central Europe, *Global Biogeochem. Cycles*, 27(3), 828–835, doi:10.1002/gbc.20071,
1022 2013a.

1023

1024 Hoffmann, T., Mudd, S. M., van Oost, K., Verstraeten, G., Erkens, G., Lang, a., Middelkoop, H., Boyle, J., Kaplan, J. O.,
1025 Willenbring, J. and Aalto, R.: Short Communication: Humans and the missing C-sink: erosion and burial of soil carbon
1026 through time, *Earth Surf. Dyn.*, 1(1), 45–52, doi:10.5194/esurf-1-45-2013, 2013b.

1027

1028 Hurtt, G. C., Chini, L. P., Frolking, S., Betts, R. A., Feddema, J. and Fischer, G.: Harmonization of land-use scenarios for
1029 the period 1500 – 2100 : 600 years of global gridded annual land-use transitions , wood harvest , and resulting secondary
1030 lands, *Clim. Chang.*, 109, 117–161, doi:10.1007/s10584-011-0153-2, 2011.

1031

1032 Kinnell, P. I. A.: Runoff dependent erosivity and slope length factors suitable for modelling annual erosion using the
1033 Universal Soil Loss Equation. *Hydrological Processes: An International Journal*, 21(20), 2681-2689, 2007.

1034

1035 Krinner, G., Viovy, N., de Noblet-Ducoudré, N., Ogée, J., Polcher, J., Friedlingstein, P., Ciais, P., Sitch, S. and Prentice, I.
1036 C.: A dynamic global vegetation model for studies of the coupled atmosphere-biosphere system, *Global Biogeochem.*
1037 *Cycles*, 19(1), 1–33, doi:10.1029/2003GB002199, 2005.

1038

1039 Lal, R.: Soil erosion and the global carbon budget., *Environ. Int.*, 29(4), 437–50, doi:10.1016/S0160-4120(02)00192-7,
1040 2003.

1041

1042 Lehner, B. and Grill, G.: Global river hydrography and network routing : baseline data and new approaches to study the
1043 world ' s large river systems, *Hydrol. Process.*, 2186(April), 2171–2186, doi:10.1002/hyp.9740, 2013.

1044

1045 Li, L., Ni, J., Chang, F., Yue, Y., Frolova, N., Magritsky, D., Borthwick, A.G., Ciais, P., Wang, Y., Zheng, C. and Walling,
1046 D.E.: Global trends in water and sediment fluxes of the world's large rivers, *Science Bulletin*, 65(1), 62-69,
1047 doi:10.1016/j.scib.2019.09.012, 2020.

1048

1049 Ludwig, W. and Probst, J.-L.: River Sediment Discharge to the Oceans: Present-Day Controls and Global Budgets, *Am. J.*
1050 *Sci.*, 298(April), 265–295, 1998.

1051

1052 Lugato, E., Smith, P., Borrelli, P., Panagos, P., Ballabio, C., Orgiazzi, A., Fernandez-ugalde, O., Montanarella, L. and
1053 Jones, A.: Soil erosion is unlikely to drive a future carbon sink in Europe, *Scientific Advances*, 4(November), eaau3523,

1054 2018.
1055
1056 Martínez-mena, M., Almagro, M., García-franco, N., Vente, J. De and García, E.: Fluvial sedimentary deposits as carbon
1057 sinks : organic carbon pools and stabilization mechanisms across a Mediterranean catchment, *Biogeosciences* 16,
1058 1035–1051, 2019.
1059
1060 Mayorga, E., Seitzinger, S. P., Harrison, J. a., Dumont, E., Beusen, A. H. W., Bouwman, a. F., Fekete, B. M., Kroeze, C.
1061 and Van Drecht, G.: Global Nutrient Export from WaterSheds 2 (NEWS 2): Model development and implementation,
1062 *Environ. Model. Softw.*, 25(7), 837–853, doi:10.1016/j.envsoft.2010.01.007, 2010.
1063
1064 Müller, C., Elliott, J., Kelly, D., Arneth, A., Balkovic, J., Ciais, P., ... & Jones, C. D.: The Global Gridded Crop Model
1065 Intercomparison phase 1 simulation dataset, *Scientific data*, 6(1), 50, 2019.
1066
1067 Nadeu, E., Gobin, A., Fiener, P., van Wesemael, B. and van Oost, K.: Modelling the impact of agricultural management on
1068 soil carbon stocks at the regional scale: the role of lateral fluxes., *Glob. Chang. Biol.*, 21(8), 3181–92,
1069 doi:10.1111/gcb.12889, 2015.
1070
1071 Naipal, V., Reick, C., Pongratz, J. and Van Oost, K.: Improving the global applicability of the RUSLE model - Adjustment
1072 of the topographical and rainfall erosivity factors, *Geosci. Model Dev.*, 8(9), doi:10.5194/gmd-8-2893-2015, 2015.
1073
1074 Naipal, V., Reick, C., Van Oost, K., Hoffmann, T. and Pongratz, J.: Modeling long-term, large-scale sediment storage using
1075 a simple sediment budget approach, *Earth Surf. Dyn.*, 4, 407–423, doi:10.5194/esurf-4-407-2016, 2016.
1076
1077 Naipal, V., Ciais, P., Wang, Y., Lauerwald, R., Guenet, B. and Oost, K. Van: Global soil organic carbon removal by water
1078 erosion under climate change and land use change during AD 1850 – 2005, *Biogeosciences*, 15(July), 4459–4480,
1079 doi:https://doi.org/10.5194/bg-15-4459-2018, 2018.
1080
1081 Van Oost, K., Quine, T. a, Govers, G., De Gryze, S., Six, J., Harden, J. W., Ritchie, J. C., McCarty, G. W., Heckrath, G.,
1082 Kosmas, C., Giraldez, J. V, da Silva, J. R. M. and Merckx, R.: The impact of agricultural soil erosion on the global carbon
1083 cycle., *Science*, 318(5850), 626–9, doi:10.1126/science.1145724, 2007.
1084
1085 Van Oost, K., Verstraeten, G., Doetterl, S., Notebaert, B., Wiaux, F. and Broothaerts, N.: Legacy of human-induced C
1086 erosion and burial on soil – atmosphere C exchange, *PNAS*, 109(47), 19492–19497,
1087 doi:10.1073/pnas.1211162109/-/DCSupplemental.www.pnas.org/cgi/doi/10.1073/pnas.1211162109, 2012.
1088
1089 Palmieri, A., Martino, L., Dominici, P. and Kasanko, M.: Land Cover and Land Use Diversity Indicators in LUCAS 2009

1088 data., 2011.

1089

1090 Panagos, P., Borrelli, P., Poesen, J., Ballabio, C., Lugato, E., Meusburger, K., Montanarella, L. and Alewell, C.:
1091 Environmental Science & Policy The new assessment of soil loss by water erosion in Europe, *Environ. Sci. Policy*, 54,
1092 438–447, doi:10.1016/j.envsci.2015.08.012, 2015.

1093

1094 Panagos, P., Borrelli, P., Meusburger, K., Yu, B., Klik, A., Lim, K. J., Yang, J. E., Ni, J., Miao, C., Chattopadhyay, N.,
1095 Sadeghi, S. H., Hazbavi, Z., Zabihi, M., Larionov, G. A., Krasnov, S. F., Gorobets, A. V., Levi, Y., Erpul, G., Birkel, C.,
1096 Hoyos, N., Naipal, V., Oliveira, P. T. S., Bonilla, C. A., Meddi, M., Nel, W., Al Dashti, H., Boni, M., Diodato, N., Van
1097 Oost, K., Nearing, M. and Ballabio, C.: Global rainfall erosivity assessment based on high-temporal resolution rainfall
1098 records, *Sci. Rep.*, 7(1), doi:10.1038/s41598-017-04282-8, 2017.

1099

1100 Parton, W. J., Schimel, D. S., Cole, C. V. and Ojima, D. S.: Analysis of Factors Controlling Soil Organic Matter Levels in
1101 Great Plains Grasslands1, *Soil Sci. Soc. Am. J.*, 51(5), 1173, doi:10.2136/sssaj1987.03615995005100050015x, 1987.

1102

1103 Pelletier, J. D.: A spatially distributed model for the long-term suspended sediment discharge and delivery ratio of drainage
1104 basins, *J. Geophys. Res., Earth Surface* 117 (F2), doi: <https://doi.org/10.1029/2011JF002129>, 2012.

1105

1106 Pelletier, J. D., Broxton, P. D., Hazenberg, P., Zeng, X., Troch, P. A., Niu, G. Y., Williams, Z., Brunke, M. A. and Gochis,
1107 D.: A gridded global data set of soil, intact regolith, and sedimentary deposit thicknesses for regional and global land
1108 surface modeling, *J. Adv. Model. Earth Syst.*, doi:10.1002/2015MS000526, 2016.

1109

1110 Peng, S., Ciais, P., Maignan, F., Li, W., Chang, J., Wang, T. and Yue, C.: Sensitivity of land use change emission estimates
1111 to historical land use and land cover mapping, *Global Biogeochem. Cycles*, 31(4), 626–643, doi:10.1002/2015GB005360,
1112 2017.

1113

1114 Renard, K. G., & Ferreira, V. A.: RUSLE model description and database sensitivity. *Journal of environmental quality*,
1115 22(3), 458-466, 1993.

1116

1117 Renard, K.G., Foster, G.R., Weesies, G.A., McCool, D.K., Yoder, D. C.: *Predicting Soil Erosion by Water: A Guide to*
1118 *Conservation Planning with the Revised Universal Soil Loss Equation (RUSLE)*, United States Department of Agriculture,
1119 Washington, DC., 1997.

1120

1121 Van Rompaey, A.J., Verstraeten, G., Van Oost, K., Govers, G. and Poesen, J.: Modelling mean annual sediment yield using
1122 a distributed approach, *Earth Surface Processes and Landforms*, 26(11), 1221-1236, 2001.

1123
1124 Schauburger, B., Ben-ari, T., Makowski, D., Kato, T., Kato, H. and Ciais, P.: Yield trends , variability and stagnation
1125 analysis of major crops in France over more than a century, *Sci. Rep.*, (November), 1–12,
1126 doi:10.1038/s41598-018-35351-1, 2018.
1127
1128 Shangguan H.W., Dai Y., Duan Q., Liu B., Y. H.: A global soil data set for earth system modeling *Wei, J. Adv. Model.*
1129 *Earth Syst.*, 6, 249–263, 2014, doi:10.1002/2013MS000293.
1130
1131 Sorribas, M. V., da Motta Marques, D., Castro, N. M. D. R., & Fan, F. M.: Fluvial carbon export and CO2 efflux in
1132 representative nested headwater catchments of the eastern La Plata River Basin, *Hydrological processes*, 31(5), 995-1006,
1133 2017.
1134
1135 Stallard, R. F.: Terrestrial sedimentation and the carbon cycle : Coupling weathering and erosion to carbon burial, *Global*
1136 *Biogeochem. Cycles*, 12(2), 231–257, 1998.
1137
1138 Tan, Z., Leung, L. R., Li, H., Tesfa, T., Vanmaercke, M., Poesen, J., ... Hartmann, J. A Global data analysis for representing
1139 sediment and particulate organic C carbon yield in Earth System Models. *Water Resources Research*, 53, 10,674–10,700.
1140 <https://doi.org/10.1002/2017WR020806>, 2017
1141
1142 Thonicke, K., Spessa, A., Prentice, I. C., Harrison, S. P. and Dong, L.: The influence of vegetation , fire spread and fire
1143 behaviour on biomass burning and trace gas emissions: results from a process-based model, *Biogeosciences*, 7,
1144 1991–2011, doi:10.5194/bg-7-1991-2010, 2010.
1145
1146 Todd-Brown, K. E., Randerson, J. T., Post, W. M., Hoffman, F. M., Tarnocai, C., Schuur, E. A., & Allison, S. D.: Causes of
1147 variation in soil carbon simulations from CMIP5 Earth system models and comparison with observations, *Biogeosciences*
1148 (10), 1717-1736, 10.5194/bg-10-1717-2013, 2013.
1149
1150 Wang, Z., Govers, G., Steegen, A., Clymans, W., Putte, A. Van Den, Langhans, C., Merckx, R. and Oost, K. Van:
1151 Geomorphology Catchment-scale carbon redistribution and delivery by water erosion in an intensively cultivated area,
1152 *Geomorphology*, 124(1–2), 65–74, doi:10.1016/j.geomorph.2010.08.010, 2010.
1153
1154 Wang, Z., Doetterl, S., Vanclooster, M., van Wesemael, B. and Van Oost, K.: Constraining a coupled erosion and soil
1155 organic carbon model using hillslope-scale patterns of carbon stocks and pool composition, *J. Geophys. Res.*
1156 *Biogeosciences*, 120, 452–465, doi:10.1002/2014JG002768, 2015.
1157
1158 Wang, Z., Hoffmann, T., Six, J., Kaplan, J. O., Govers, G., Doetterl, S. and Van Oost, K.: Human-induced erosion has

1159 offset one-third of carbon emissions from land cover change, Nat. Clim. Chang., 7(5), 345–349, doi:10.1038/nclimate3263,
1160 2017.

1161

1162 Wiesmeier, M., Sporlein, P., Geuß, U. W. E., Hangen, E., Haug, S., Reischl, A., Schilling, B., Lutzow, M. V. O. N. and
1163 Kogel-Knaber, I.: Soil organic carbon stocks in southeast Germany (Bavaria) as affected by land use , soil type and
1164 sampling depth, Glob. Chang. Biol., (March), 1–13, doi:10.1111/j.1365-2486.2012.02699.x, 2012.

1165

1166

1167

1168

1169

1170

1171

1172

1173

1174

1175

1176

1177

1178

1179

1180

1181

1182

1183

1184

1185

1186

1187

1188

1189

1190

1191

1192

1193 **Table 1:** Model input datasets

Dataset	Spatial resolution	Temporal resolution	Period	Source
Historical land cover and land use change	0.25 degrees	annual	1850-2005	Peng et al. (2017)
Climate data (precipitation & temperature) for ORCHIDEE	0.5 degrees	6 hourly	1900-2012	CRU-NCEP version 5.3.2; https://crudata.uea.ac.uk/cru/data/ncep/ ; last access: 5 April 2019
precipitation for the Adj. RUSLE	0.5 degrees	monthly	1850-2005	ISIMIP2b (Frieler et al., 2017)
Soil	1 km	-	-	Global Soil Dataset for Earth System Modeling, GSDE (Shangguan H.W., Dai Y., Duan Q., Liu B., 2014)
Topography	30 arcseconds	-	-	GTOPO30; U.S. Geological Survey, EROS Data Center Distributed Active Archive Center 2004; https://www.ngdc.noaa.gov/mgg/topo/gltiles.html ; last access: 5 April 2019
Flow accumulation	30 arcseconds	-	-	HydroSHEDS (Lehner et al., 2013); https://www.hydrosheds.org/ ; last access: 5 April 2019
Hillslopes/Floodplain area	5 arcminutes	-	-	Pelletier et al. (2016)
River network & stream length	30 arcseconds	-	-	Hydrosheds (Lehner et al., 2008)

1194

1195

1196

Table 2: Model simulations, with changes to the basin average gross soil erosion rate ($t\ ha^{-1}\ y^{-1}$), the basin average sediment residence time Tau (years), and the enrichment factor, and the crop residue harvest intensity, RM (%).

Default simulations	Gross soil erosion	Tau	Enrichment factor	RM
S0	0	-	-	0
S1	3.94	94	1	0
S2	3.94	94	1	0
Uncertainty simulations				
S1_min	1.52	94	1	0
S2_min	1.52	94	1	0
S1_max	5.95	94	1	0

S2_max	5.95	94	1	0
Sensitivity simulations				
S2_Tmin	3.94	60	1	0
S2_Tmax	4.94	128	1	0
S1_EF	5.94	94	2	0
S2_EF	6.94	94	2	0
S0_RM	0	-	-	100
S1_RM	3.94	94	1	100
S2_RM	3.94	94	1	100

1197
1198 **Table 3:** Goodness-of-fit results of the comparison of the simulated gross and net erosion rates to those of other studies at
1199 subbasin level, taking into account 13 sub-basins of the Rhine. RMSE is the root mean square error in 10^6 tons year⁻¹. E
1200 stands for soil erosion.

	E Cerdan et al. (2010)	E Germany	E RUSLE2015	E Borrelli et al. (2018)
<i>r-squared</i>	0.72	0.97	0.94	0.24
<i>RMSE</i>	0.68	1.98	0.92	1.35

1201
1202 **Table 4:** Goodness-of-fit results of the comparison of the simulated gross and net C erosion rates to those of the study of
1203 Lugato et al. (2018) in the enhanced and reduced scenario, taking into account 13 sub-basins of the Rhine. RMSE is the
1204 root mean square error in tons year⁻¹. Ce stands for gross C erosion, while Cd stands for net C erosion.

	Ce enhanced	Ce reduced	Cd enhanced	Cd reduced
<i>r-squared</i>	0.95	0.95	0.98	0.98
<i>RMSE</i>	7977	13797	3450	9822

1205
1206 **Table 5:** This table shows the results of the linear regression between the simulated total SOC stocks (Tg of C per year)
1207 and those of the Global Soil dataset for Earth System Modeling (GSDE) and from the LUCAS database. The regression is
1208 done after aggregating the data at sub-basin level for the 13 sub-basins that were delineated in the Rhine catchment.
1209 RMSE is the root mean square error given in Tg of C per year, while the r-value is the spatial correlation coefficient.

Regression	r-value	p-value	RMSE
This study versus LUCAS	0.96	<0.01	28.69

This study versus GSDE	0.95	<0.01	29.32
------------------------	------	-------	-------

1210
1211 **Table 6:** This table presents the scaling exponent (b) of equation 20 for floodplains and hillslopes. The scaling exponent
1212 was derived for selected points in the Rhine catchment for which measurements on the SOC storage were taken by
1213 Hoffmann et al. (2013), and at sub-basin level after the data on area and SOC stocks was aggregated for each of the 13
1214 sub-basins of the Rhine.

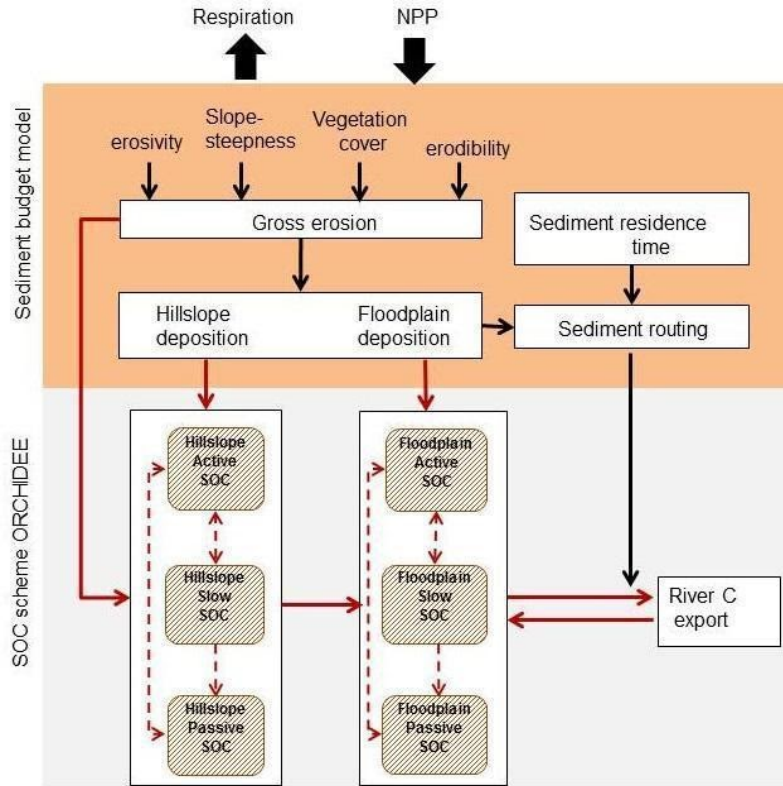
	Scaling exponent floodplains	Scaling exponent hillslopes
Hoffmann et al. (2013)	1.23±0.06	1.08±0.07
This study (selected points where measurements were taken)	1.14	0.83
This study (based on the 13 sub-basins)	1.06	1.00

1215
1216 **Table 7:** Sensitivity analysis. The impacts of enrichment, changes to the sediment residence time (τ_{min} , τ_{max}), and crop
1217 residue management (RM) on the cumulative gross C erosion (C_e), the cumulative change in the total SOC stock ($dSOC$), the
1218 net C sink and the cumulative particulate organic C export flux (POC_{exp}) of the Rhine catchment. Units: Tg C

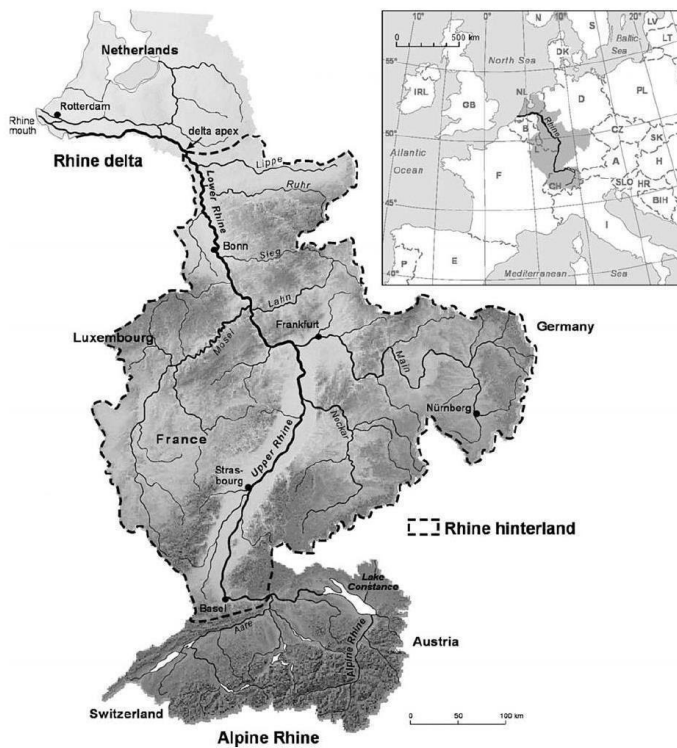
	C_e	$dSOC$	C sink/source	POC_{exp}
Default	66	142	216	0.029
enrichment	106	198	271	0.032
τ_{min}	66	130	204	0.026
τ_{max}	66	100	173	0.036
RM	52	105	194	0.031

1219

1220

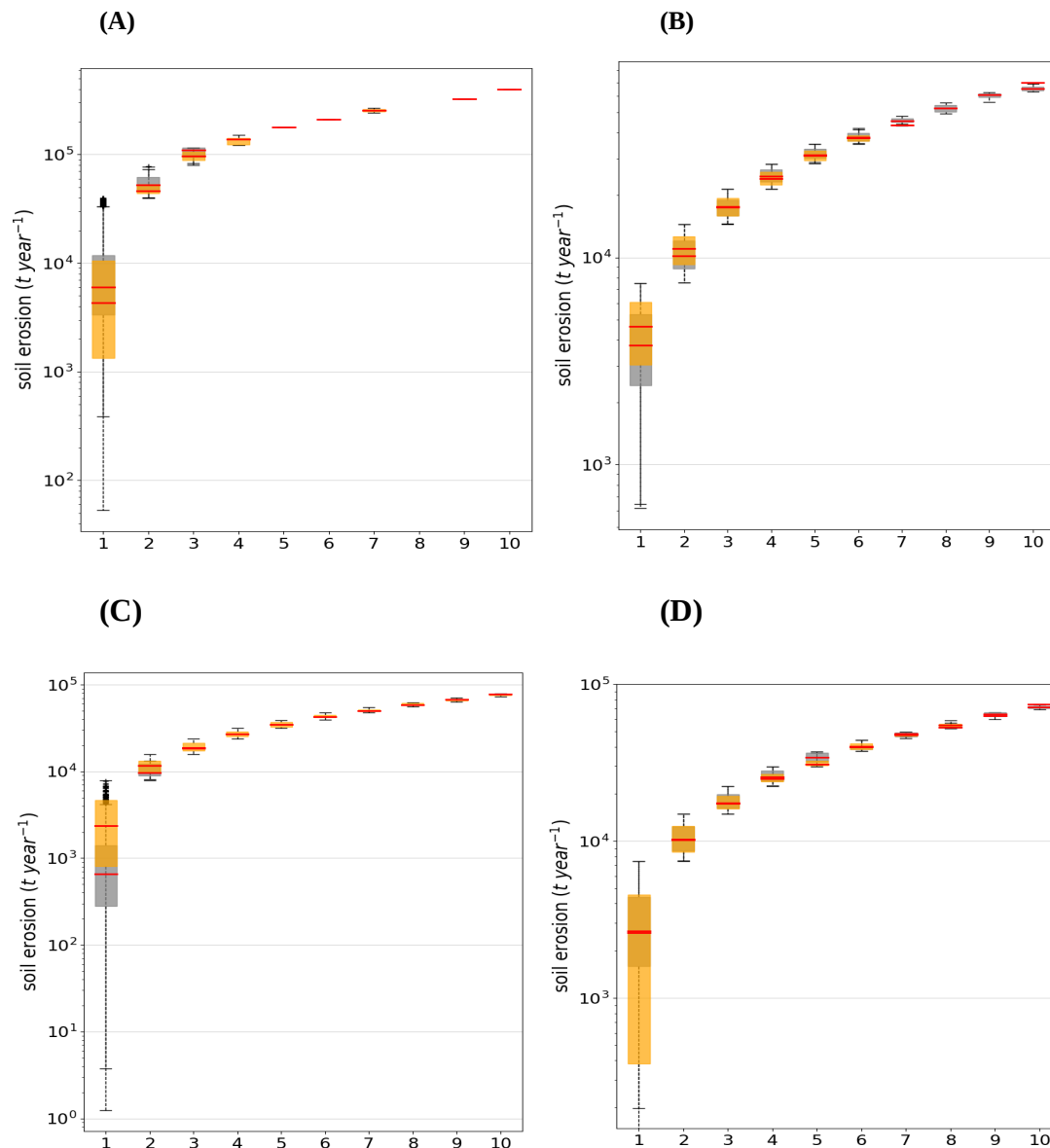


1221 **Figure 1:** A conceptual diagram of CE-DYNAM. The red arrows represent the C fluxes between the C pools/reservoirs,
 1222 while the black arrows represent the link between the erosion processes (removal, deposition and transport).
 1223



1224 **Figure 2:** The Rhine catchment (Hoffmann et al., 2013), where the gray shades represent elevation and the continuous
1225 black lines the main rivers.

1226
1227



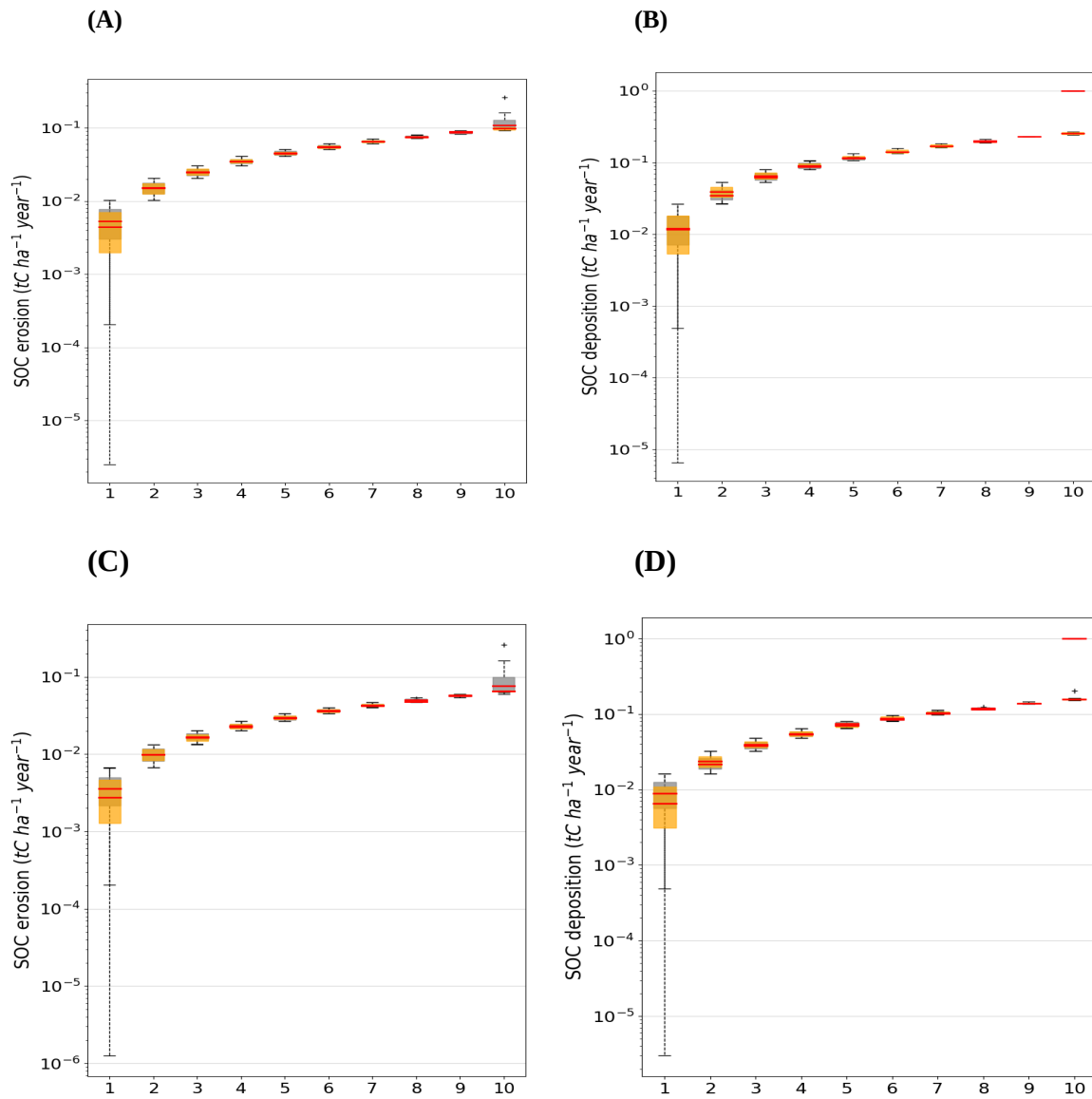
1228
1229

1230 **Figure 3:** Quantile-whisker plot of simulated **gross** soil erosion rates (t/year) (grey whisker boxes), compared to (A) the
1231 study of Cerdan et al. (2010), (B) the study of Panagos et al. (2015), and (C) the German potential erosion map by Bug et
1232 al. (2014) (orange whisker boxes). (D) Quantile-whisker plot of simulated **net** soil erosion rates (t/year) (grey whisker
1233 boxes), compared to the study of Borrelli et al. (2018) (orange whisker boxes). Medians are plotted as red horizontal lines.
1234 The x-axis represents bins or evenly spaced ranges between the minimum and maximum total yearly soil erosion rates of
1235 the Rhine derived from the data of (a) Cerdan et al. (2010), (b) Panagos et al. (2015), (c) Bug et al. (2014), and (d) Borrelli
1236 et al. (2018).

1237

1238

1239

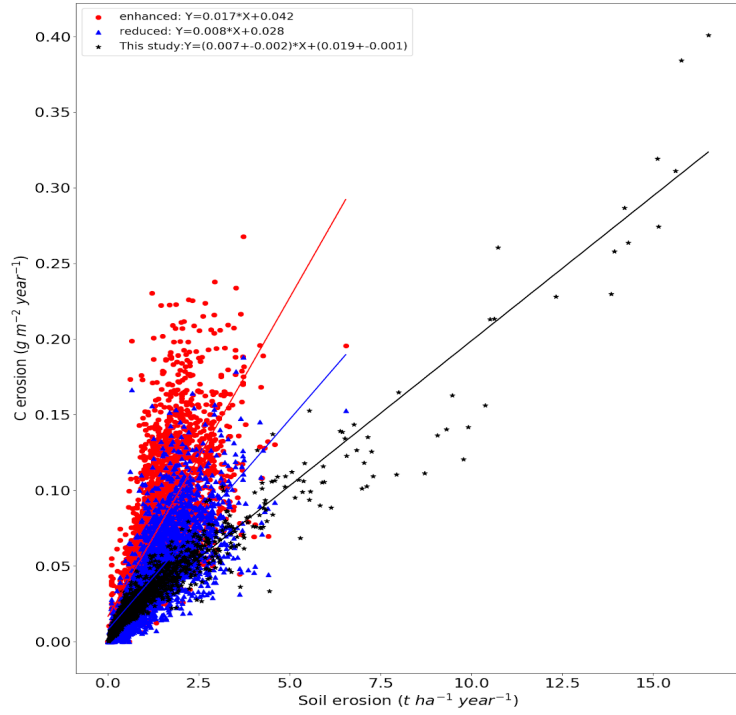


1240

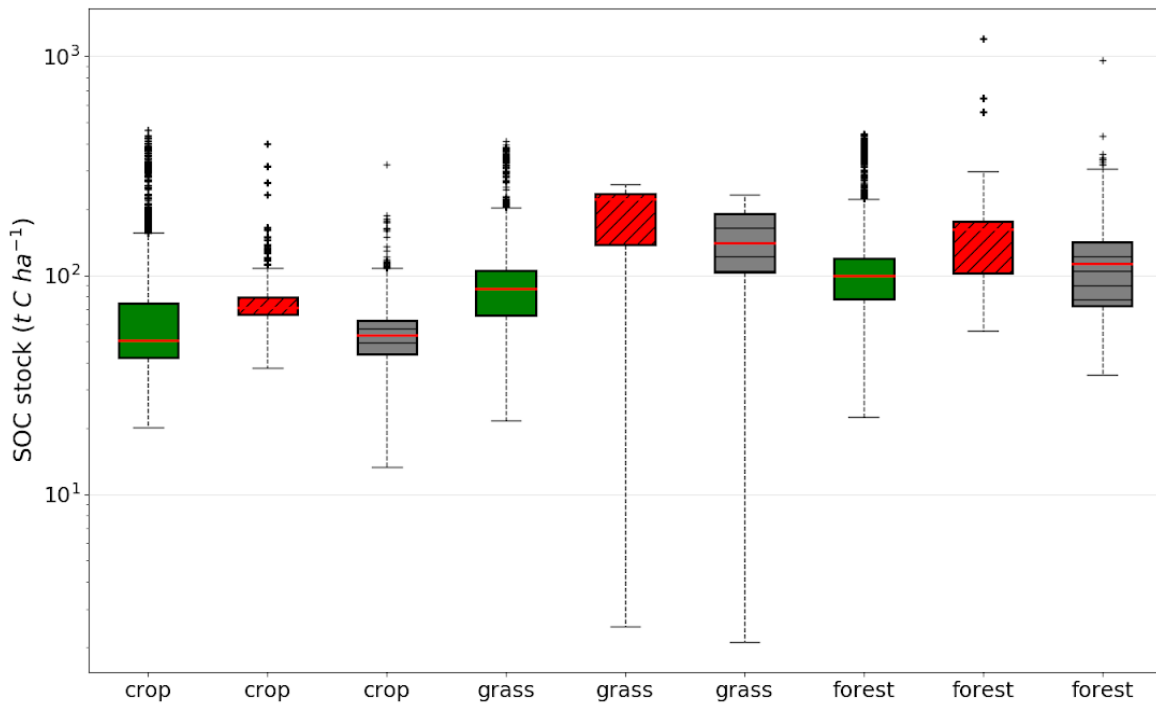
1241

1242 **Figure 4:** (A) Hillslope C erosion rates and, (B) C deposition rates, compared to the enhanced erosion scenario from
1243 Lugato et al. (2018). (C) Hillslope C erosion rates and, (D) C deposition rates, compared to the reduced erosion scenario
1244 from Lugato et al. (2018). The x-axis represents bins or evenly spaced ranges between the minimum and maximum total
1245 yearly soil erosion rates of the Rhine.

1246

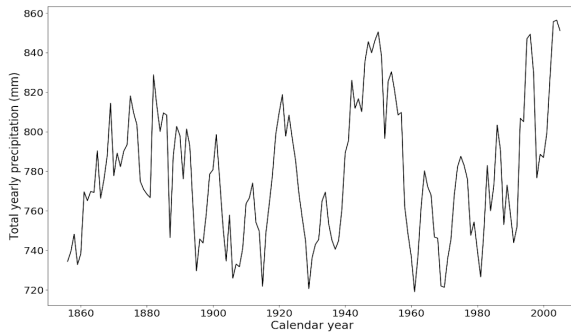


1247 **Figure 5:** The relationship between soil erosion and C erosion of simulation S2 (blackstars) in comparison to the erosion
1248 scenarios from the study of Lugato et al. (2018) with enhanced (red circles) and reduced erosion (blue triangles),
1249 respectively. The straight lines are the trendlines of the linear regression between soil and C erosion.
1250

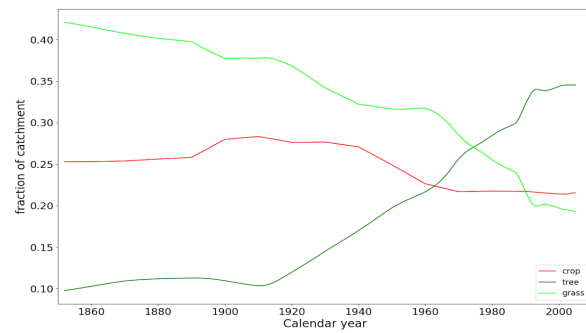


1251 **Figure 6:** Comparison of the total SOC stocks per land cover type between the simulation without erosion (red boxes with
 1252 a ‘//’ pattern), the simulation with erosion (black boxes with a ‘-’ pattern) and the LUCAS data (green boxes without
 1253 pattern fill). The red horizontal lines are the medians, the dashed vertical lines represent the range between the minimum
 1254 and maximum, and the black dots are the outliers.

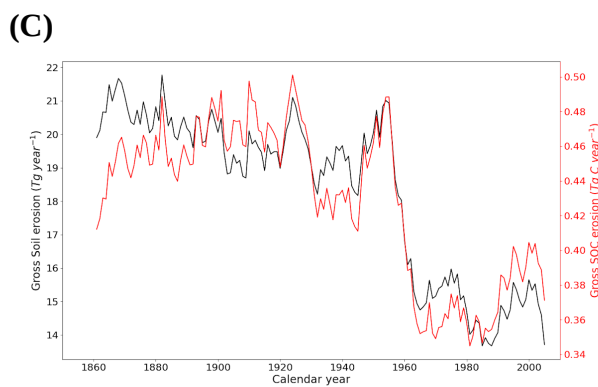
1255 (A)
 1256



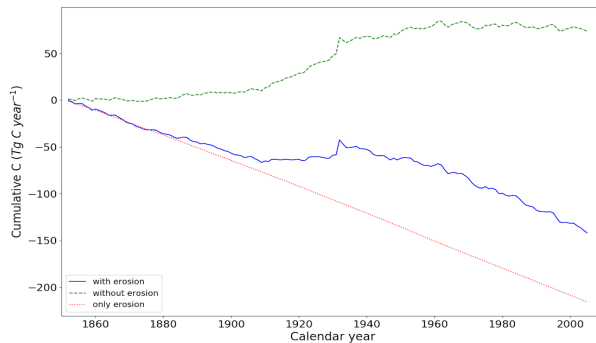
(B)



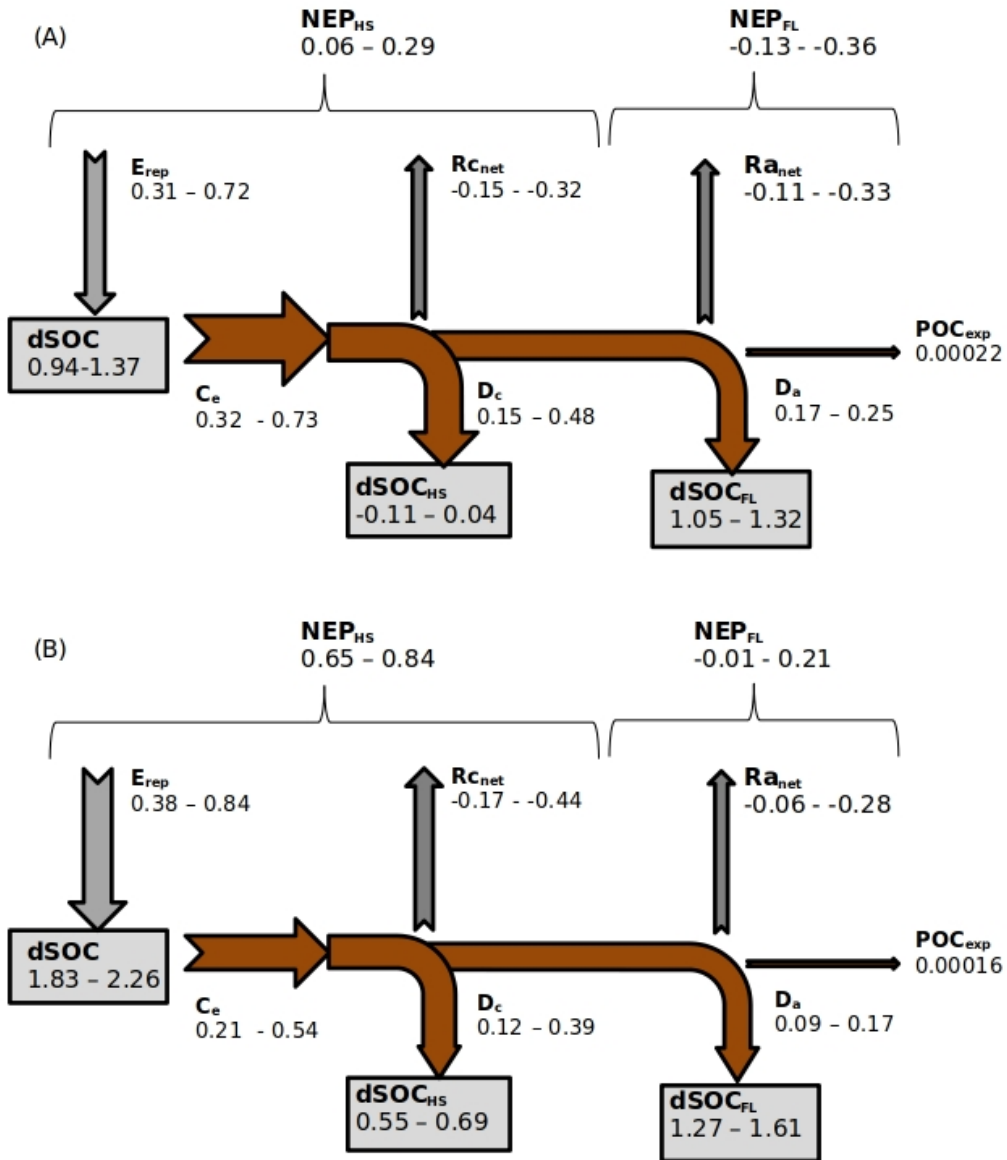
1257 (C)
 1258



(D)



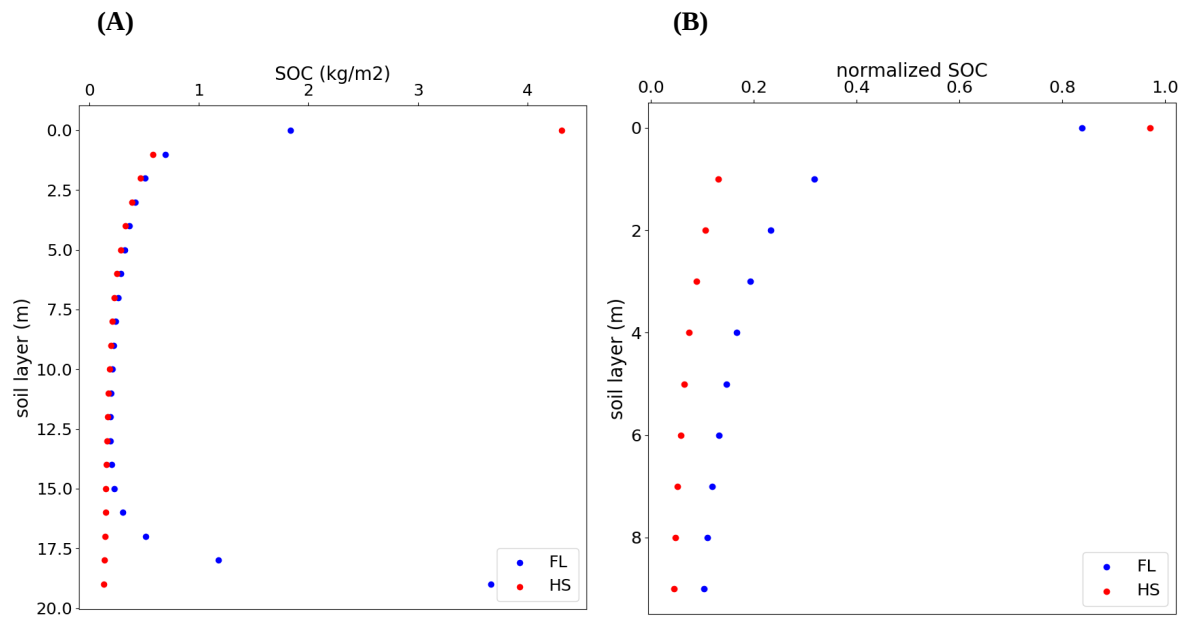
1259 **Figure 7:** Timeseries of (A) the 5-year average yearly precipitation (mm), (B) changing land cover fractions, (C): 5-year
 1260 average total gross soil erosion (Pg year^{-1}) and total gross C erosion rates (Tg C year^{-1}), (D): Cumulative C emissions from
 1261 the soil to the atmosphere under land use change and climate change without soil erosion (green dashed line), with soil
 1262 erosion (blue straight line), due to additional respiration or stabilization of buried soil and photosynthetic replacement of C
 1263 under erosion (E_p , red dotted line). All graphs represent the non-Alpine region of the Rhine catchment.



1265 **Figure 8:** (A) C budget of the non-Alpine part of the Rhine for the period 1851-1861, and (B) for the period 1995-2005.
 1266 The budget shows the net exchange of C ($Tg\ C\ year^{-1}$) between the soil and atmosphere as a result of accelerated soil
 1267 erosion rates. Grey arrows are the erosion-induced yearly average **vertical** C fluxes, while the brown arrows are the
 1268 erosion-induced yearly average **lateral** C fluxes. C_e : Gross C erosion from hillslopes; D_c : Deposition of C on hillslopes;
 1269 D_a : Deposition of C in floodplains; POC_{exp} : net POC export flux; E_p : Erosion-induced C replacement on hillslopes (Eq. 21);
 1270 $R_{a_{net}}$: Net respiration/burial of deposited C in floodplains (Eq. 23); $R_{c_{net}}$: Net respiration/burial of deposited C on hillslopes
 1271 (Eq. 22); NEP_{HS} : Net ecosystem productivity of hillslopes; NEP_{FL} : Net ecosystem productivity of floodplains; The grey
 1272 boxes represent yearly average changes in SOC stocks for the specific time period as a result of land use change, climate

1273 change, erosion and deposition. $dSOC$: Yearly average change in the total SOC stock; $dSOC_{HS}$: Yearly average change in
1274 the hillslope SOC stock; $dSOC_{FL}$: Yearly average change in the floodplain SOC stock.

1275
1276



1277 **Figure 9:** (A) Vertical distribution of hillslope (red) and floodplain (blue) SOC stocks (kg m^{-2}) with depth averaged over
1278 the non-Alpine region of the Rhine catchment, and (B) the vertical distribution of normalized hillslope (red) and floodplain
1279 (blue) SOC stocks (dimensionless) with depth.